

## Single Agents with Designed Combination Chemotherapy Potential: Synthesis and Evaluation of Substituted Pyrimido[4,5-*b*]indoles as Receptor Tyrosine Kinase and Thymidylate Synthase Inhibitors and as Antitumor Agents

Aleem Gangjee,<sup>\*,†</sup> Nilesh Zaware,<sup>†</sup> Sudhir Raghavan,<sup>†</sup> Michael Ihnat,<sup>‡</sup> Satyendra Shenoy,<sup>‡</sup> and Roy L. Kisliuk<sup>§</sup>

<sup>†</sup>*Division of Medicinal Chemistry, Graduate School of Pharmaceutical Sciences, Duquesne University, 600 Forbes Avenue, Pittsburgh, Pennsylvania 15282*, <sup>‡</sup>*Department of Cell Biology, The University of Oklahoma Health Science Center, Oklahoma City, Oklahoma 73104*, and <sup>§</sup>*Department of Biochemistry, Tufts University School of Medicine, 136 Harrison Avenue, Boston, Massachusetts 02111*

Received July 27, 2009

Combinations of antiangiogenic agents (AAs) with cytotoxic agents have shown significant promise in cancer treatment, and several such clinical trials are currently underway. We have designed, synthesized, and evaluated two compounds that each inhibit vascular endothelial growth factor receptor-2 (VEGFR-2) and platelet-derived growth factor receptor- $\beta$  (PDGFR- $\beta$ ) for antiangiogenic effects and also inhibit human thymidylate synthase (hTS) for cytotoxic effects in single agents. The synthesis of these compounds involved the nucleophilic displacement of the common intermediate 5-chloro-9H-pyrimido[4,5-*b*]indole-2,4-diamine with appropriate benzenethiols. The inhibitory potency of both these single agents against VEGFR-2, PDGFR- $\beta$ , and hTS is better than or close to standards. In a COLO-205 xenograft mouse model, one of the analogs significantly decreased tumor growth (tumor growth inhibition (TGI) = 76% at 35 mg/kg), liver metastases, and tumor blood vessels compared with a standard drug and with control and thus demonstrated potent tumor growth inhibition, inhibition of metastasis, and antiangiogenic effects *in vivo*. These compounds afford combination chemotherapeutic potential in single agents.

Antiangiogenic agents (AA)<sup>a</sup> have established a new paradigm in cancer chemotherapy and have allowed significant progress toward the control and treatment of various cancers.<sup>1</sup> Normal cell angiogenesis is initiated under conditions of injured or hypoxic tissues, occurs in wound healing, menstrual cycle and pregnancy, and is promoted by vascular endothelial growth factor (VEGF) and similar growth factors. Except for these conditions, angiogenesis is mostly absent in normal tissues.<sup>2</sup> Heterogeneous solid growing tumors however are in a state of angiogenesis and continually overexpress growth factors.

Receptor tyrosine kinases (RTKs) are a subclass of cell surface growth factor receptors with intrinsic, ligand-controlled tyrosine kinase activity.<sup>3,4</sup> Epidermal growth factor

receptor (EGFR), platelet-derived growth factor receptor (PDGFR), and vascular endothelial growth factor receptor (VEGFR) families of receptors are all RTKs and, despite their diverse biological roles, share similarities in structure and domain arrangement.

Clinically useful RTK inhibitors have resulted from small molecule ATP competitive inhibitors (Figure 1) that target the kinase domain of RTKs. While RTK inhibitors have afforded a new mechanism for the treatment of a variety of cancers, it was quickly realized that single RTK inhibitors allowed the development of resistance by point mutations in the ATP binding site. In addition, the molecular pathways responsible for tumor growth, survival, and metastasis are redundant and adaptable between individual patients and within tumors in the same patient. Thus treatment targeting a single RTK would be highly unlikely to provide long-term tumor control in most patients. Proangiogenic growth factors are redundantly expressed by both tumor and stromal cells.<sup>5</sup> Thus there is now a paradigm shift in the utility of RTK inhibitors for cancer treatment in that rather than single RTK inhibition it is now desirable to use multitargeted RTK inhibitors to overcome possible resistance and thwart the escape mechanism of alternative pathways for tumor growth. Recent FDA approvals of just such multitargeted RTK inhibitors sorafenib (VEGFR-2, PDGFR- $\beta$ , FMS-like tyrosine kinase 3 (Flt-3), raf kinase, and stem cell factor receptor (c-kit)) and sunitinib (VEGFR-1, -2, and -3, PDGFR- $\beta$  and - $\alpha$ , Flt-3, and colony stimulating factor 1 receptor (CSF-1R)) attest to the importance of this new paradigm in cancer chemotherapy.<sup>3–12</sup>

\*To whom correspondence should be addressed. Telephone: 412-396-6070. Fax: 412-396-5593. E-mail address: gangjee@duq.edu.

<sup>a</sup>Abbreviations: AA, antiangiogenic agents; VEGF, vascular endothelial growth factor; RTK, receptor tyrosine kinases; EGFR, epidermal growth factor receptor; PDGFR, platelet-derived growth factor receptor; *abl*, abelson proto-oncogene; c-kit, stem cell factor receptor; CSF-1R, colony stimulating factor 1 receptor; Flt-3, FMS-like tyrosine kinase 3; ErbB-2, human epidermal growth factor receptor 2; hTS, human thymidylate synthase; hDHFR, human dihydrofolate reductase; GARFT, glycinamide-ribonucleotide formyl transferase; AICARFT, aminoimidazole-4-carboxamide-ribonucleotide formyl transferase; 5-FU, 5-fluorouracil; PMX, pemetrexed; RTX, raltitrexed; MTX, methotrexate; TMQ, trimetrexate; PDB, protein data bank; DMSO<sub>2</sub>, methyl sulfone; DMAP, 4-dimethylaminopyridine; DMF, dimethylformamide; POCl<sub>3</sub>, phosphorus oxychloride; NMP, *N*-methyl-2-pyrrolidone; PI3K, phosphatidylinositol 3-kinase; CAM, chorioallantoic membrane; TGI, tumor growth inhibition; MTD, maximum tolerated dose; ADR, adverse drug reaction.

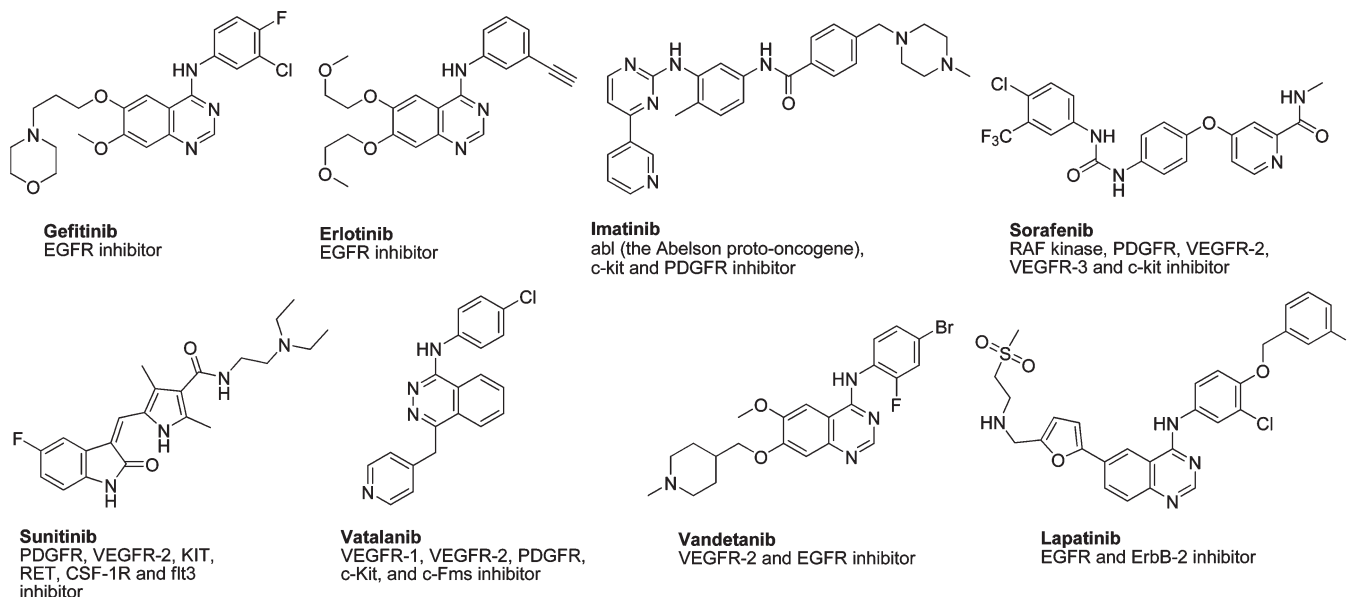


**Figure 1.** Single and multitargeted RTK inhibitors.

In addition, vandetanib is a VEGFR-2 inhibitor that combines EGFR (rather than PDGFR- $\beta$ ) inhibitory activity, and lapatinib also combines EGFR and human epidermal growth factor receptor-2 (ErbB-2) inhibitory activity. All of these multitargeting RTK inhibitors have some monotherapy potential but are mostly cytostatic (some cytotoxicity has been observed via apoptosis in a limited number of tumor types); thus for optimal benefit they must be combined with cytotoxic, conventional chemotherapeutic agents, radiation therapy, or both.<sup>13</sup> The rationale and mechanisms for the success of these combinations continues to provide discussion in the literature.<sup>13,14</sup> Hundreds of such ongoing clinical trials (clinicaltrials.gov) attest to the importance of the concept and the individual drugs, both cytostatic and cytotoxic, in the combinations.

Combination therapy with VEGFR-2 (endothelial cell inhibition) along with PDGFR- $\beta$  inhibition (pericytes inhibition) increases the antiangiogenic effect even in the often intractable late state of solid tumors.<sup>15,16</sup> Thus targeting both VEGFR-2 and PDGFR- $\beta$  simultaneously is a desirable goal for AAs that have cytostatic and perhaps cytotoxic activity. The clinical success of sunitinib<sup>9,11</sup> and sorafenib<sup>11</sup> that target both VEGFR and PDGFR attests to the viability of this combination in single agent multi-RTK inhibitors. Preclinical and clinical evidence indicates that combinations of AAs with conventional cytotoxic agents, radiation therapy, or both results in additive or even synergistic antitumor effects<sup>15–17</sup> and that monotherapy is usually unsuccessful with antiangiogenic agents. Rapid vascular regrowth in tumors after the removal of AAs attests to their cytostatic mechanism.<sup>18,19</sup>

Combination cancer chemotherapy is not a new idea. Recent studies indicate that the combination of antiangiogenic agents with cytotoxic agents is more effective in cancer treatment.<sup>20</sup> However, what would be novel is if a single agent could be found that had both antiangiogenic activity by multitargeting RTKs and also possessed cytotoxic activity to afford combination chemotherapy in a single agent. We<sup>21</sup> synthesized such agents with VEGFR-2, PDGFR- $\beta$ , and dihydrofolate reductase (DHFR) inhibition with good results. However, the potency of the cytotoxic component in these agents was extremely low.<sup>21</sup> Thus we elected to structurally

engineer multi-RTK inhibitory attributes along with the deliberate design of cytotoxicity in single agents as a second iteration of our previous report. Such single agents would circumvent the pharmacokinetic problems of multiple agents, would avoid drug–drug interactions, could be used at lower doses to alleviate toxicity, could be devoid of overlapping toxicities, and could delay or prevent tumor cell resistance. Most importantly providing the cytotoxic agent, by structural design, in the same molecule allows the cytotoxicity to be manifested as soon as the antiangiogenic effects are operable. A separately dosed cytotoxic agent may miss the timing window and hence preclude the intent of the combination. Such multitargeted agents could exert their cytotoxic action as soon as or even during transient tumor vasculature normalization<sup>13,22</sup> due to the antiangiogenic effects. Thus such agents might not need to be as potent as conventional separately dosed cytotoxic agents. Dosing of such an antiangiogenic multitargeted RTK inhibitor with a built-in cytotoxic mechanism would be tantamount to providing a combination of multitargeted RTK inhibitors along with a metronomic dosing of a cytotoxic agent. Thus these single agents would be in keeping with the two important mechanisms that explain the rationale for the success of separate antiangiogenic and cytotoxic chemotherapeutic agents in combination for cancer chemotherapy.<sup>13,22–25</sup> Other advantages of such single agents are in the reduced cost and increased patient compliance, which are sometimes as significant contributors to chemotherapy failure as resistance, toxicity, and lack of efficacy.

The antiangiogenic component is usually targeted to tumor cells and is, under most circumstances, not targeted to normal cells. However, the cytotoxic component is targeted to the tumor cells but not exclusively. Thus the challenge in designing single agents with a cytotoxic component is that the cytotoxic component should be potent enough to kill tumor cells that have been compromised via the antiangiogenic effect but not potent enough to cause serious toxicity to normal cells not affected by the antiangiogenic effect. Clearly one of the problems with conventional cytotoxic chemotherapeutic agents is dose-limiting toxicities. These single agents should avoid these toxicities since they do not need to be as potent as conventional chemotherapeutic agents.

We have designed and synthesized compounds **1** and **2** (Figure 2), which each target VEGFR-2 and PDGFR- $\beta$  and provide antiangiogenic effects in vivo and also have human thymidylate synthase (hTS) inhibitory activity to afford the cytotoxic component in vivo in single agents. The choice of VEGFR-2<sup>26</sup> and PDGFR- $\beta$ <sup>27</sup> inhibition for antiangiogenic activity was obvious since these are the principal direct and indirect mediators of angiogenesis. The choice of inhibition of human dihydrofolate reductase (hDHFR) or hTS as the cytotoxic component was based in part on our long-standing interest in inhibitors of folate metabolizing enzymes and on structural, architectural, and molecular modeling considerations in the design of the molecules. In addition, the successful clinical and preclinical combinations of capecitabine,<sup>28,29</sup> 5-FU<sup>30</sup> (TS inhibitors) and pemetrexed (PMX)<sup>31,32</sup> (TS and DHFR inhibitor) (Figure 3) with AAs in combination therapy with and without radiation was also an important factor in selecting TS or DHFR as the possible cytotoxic targets in the design of **1** and **2**.

DHFR carries out the reduction of dihydrofolate to tetrahydrofolate and maintains the pool of reduced folate cofactors that function in one carbon transfers in a variety of metabolic transformations crucial for cell survival.<sup>33</sup> Thus inhibitors of DHFR such as methotrexate (MTX) and PMX (Figure 3) have found utility as antitumor agents. TS carries out the sole de novo biosynthesis of TMP from dUMP. It utilizes 5,10-methylenetetrahydrofolate as a cofactor to transfer the methyl group to dUMP.<sup>34</sup> Because of its pivotal role in DNA synthesis and cell growth, it is a viable target for several clinically used cancer chemotherapeutic agents.<sup>35</sup> The fluoropyrimidine 5-FU and its derivatives, in particular, capecitabine (Figure 3), have found extensive utility in ovarian, breast, colon, and several other cancers alone and in combinations and are a mainstay in cancer chemotherapy.<sup>36</sup> Folate-based

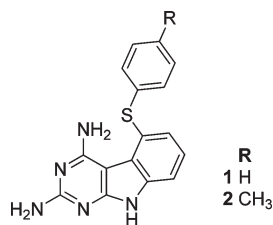


Figure 2. Target compounds **1** and **2**.

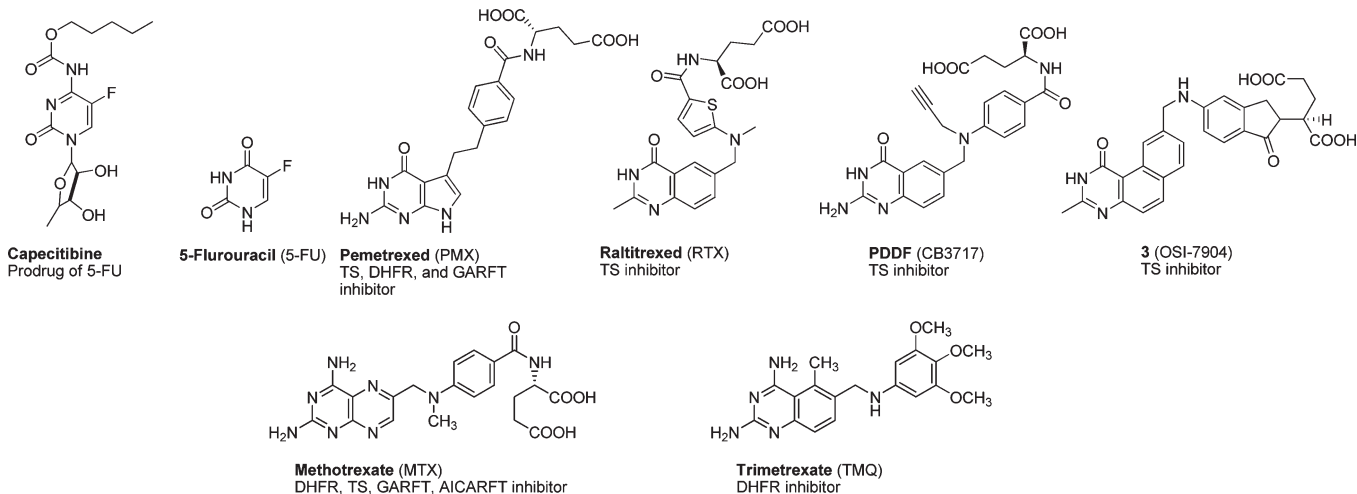
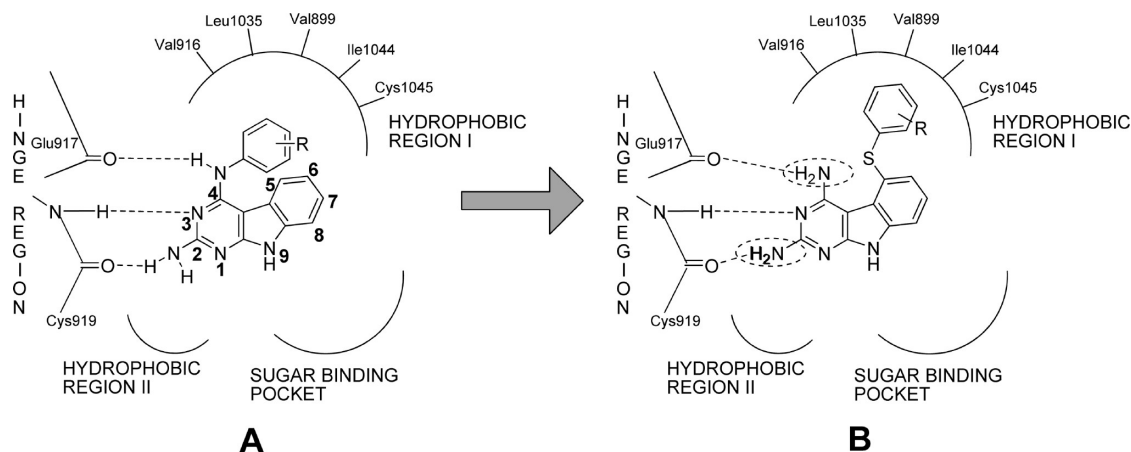


Figure 3. Dihydrofolate reductase and thymidylate synthase inhibitors.

TS inhibitor antimetabolites (Figure 3) that are clinically used alone or in combination in a variety of cancers include PMX<sup>37</sup> and in Europe raltitrexed (RTX) a derivative of PDDF. In addition, **3** (Figure 3), also a TS inhibitor, and its derivatives are in various stages of clinical development alone and in combinations against a variety of cancers.<sup>38</sup>

Tricyclic scaffolds reported in the literature with appropriate 4-anilino substitutions have shown excellent RTK inhibition.<sup>39,40</sup> An example of such an analog is presented in Figure 4A.<sup>39</sup> In a general RTK model, it was shown<sup>41–44</sup> that the 2-NH<sub>2</sub>, the N3, and the 4-anilino nitrogen of the pyrimidine ring of RTK inhibitors H-bond with the hinge region as depicted in Figure 4A. In addition, the phenyl ring of the 4-anilino moiety lies in the hydrophobic region 1, and the tricyclic scaffold mimics the purine ring of ATP.<sup>39,40</sup> We reasoned that transposing the phenyl ring from the 4-position (Figure 4A) to the 5-position of the tricyclic scaffold as shown in Figure 4B maintains access to hydrophobic region 1 and allows the H-bonds with the hinge region. Such compounds with phenyl substitutions in the 5-position should maintain RTK inhibitory activity. However, moving the phenyl ring from the 4- to the 5-position unveils a 2,4-diaminopyrimidine motif on the tricyclic scaffold (Figure 4B) that is highly conducive for DHFR or TS inhibition or both.<sup>45,46</sup> MTX and trimetrexate (TMQ) (Figure 3) are well-known 2,4-diamino fused pyrimidines with hDHFR inhibition and for MTX hTS inhibitory activity as well.<sup>47</sup> Usually DHFR and TS inhibitors have a 2,4-diamino and a 2-amino-4-oxo substitution on the pyrimidine ring, respectively. There are however reports where analogs with a 2,4-diamino substitution have TS and DHFR inhibitory activity<sup>45,46</sup> while a 2-amino-4-oxo substitution provides DHFR and TS inhibitory activity.<sup>48,49</sup> Thus we designed 2,4-diamino-5-thio phenyl substituted pyrimido[4,5-*b*]indoles as potential RTK inhibitors with DHFR or TS inhibitory attributes or both.

Molecular modeling with hDHFR confirmed that the third ring of the tricyclic scaffold could afford additional interaction with Ile60 of hDHFR<sup>50</sup> over the previously synthesized bicyclic analogs.<sup>21</sup> Modeling (Figure 5) using SYBYL7.3<sup>51</sup> and superimposition of one of the energy-minimized conformations of **1** with the pyrimidine ring of **1** on the X-ray crystal structure of the pyrimidine ring of the pyrido[2,3-*d*]pyrimidine inhibitor (not shown) (1PDB)<sup>50</sup> in hDHFR shows that the 2,4-diamino motif is maintained for hDHFR inhibitory



**Figure 4.** Rationale for the synthesis of target molecules.

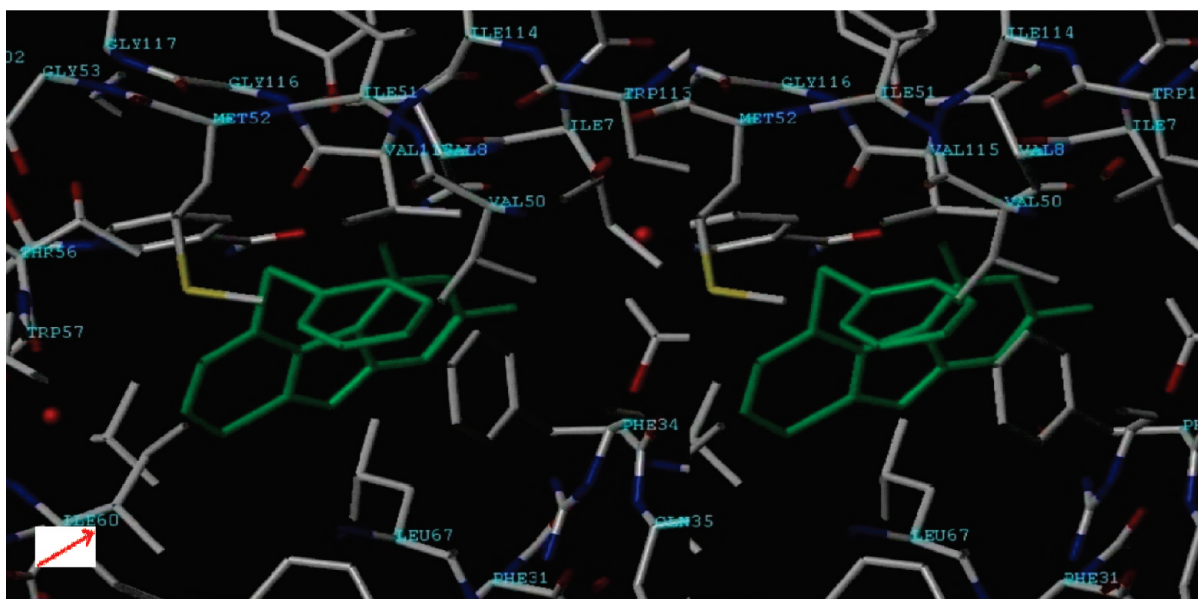


**Figure 5.** Stereoview (SYBYL7.3) of the pyrimidine ring of **1** superimposed on the pyrimidine ring of the DHFR inhibitor in the X-ray crystal structure of hDHFR (1PDB).<sup>50</sup>

activity as is the S-Ph, which mimics the phenyl ring of MTX<sup>52,53</sup> and TMQ.<sup>50</sup> The 2NH<sub>2</sub> and N1 make a salt bridge with Glu30 in hDHFR and the S-Ph ring makes hydrophobic contact with Phe31 and Val115 much like TMQ and MTX and the third ring of the tricyclic scaffold contacts Ile60. The conformation of the phenyl ring of **1** in Figure 5 is not the usual conformation of this ring in other reported hDHFR inhibitors. With this exception all other interactions of the scaffold of **1** were similar to the pteridine of MTX and the quinazoline of TMQ. Thus we anticipated DHFR inhibitory activity for **1**.

For TS inhibitory activity, modeling **1** by superimposing the pyrimidine ring of the energy minimized **1** (yellow) onto the pyrimidine ring of the X-ray crystal structure of PMX (green) in hTS (PDB 1JU6),<sup>54</sup> Figure 6 (SYBYL 7.3), showed that the superimposition is perfect for the two scaffolds. In the molecular modeling, the hydrophobic interactions of the tricyclic C-ring of **1** with Trp109 (bottom right) are somewhat better than those of the bicyclic B-ring of PMX. In addition, the S-phenyl ring of **1** and its close proximity to the benzoyl ring of PMX (green) is evident, as are the hydrophobic interactions with Ile108, Leu221, and Phe225 (top center) (and Met311 not shown). Also evident is the stacking

interaction of **1** and dUMP (directly below **1**). Thus on the basis of molecular modeling, we anticipated compound **1** to have DHFR or TS inhibitory activity or both.

In Figure 7, energy-minimized **1** was superimposed (SYBYL7.3) onto a furo[2,3-*d*]pyrimidine<sup>55</sup> inhibitor (not shown) of VEGFR-2 in the X-ray crystal structure of VEGFR-2 (PDB 1YWN)<sup>55</sup> that indicated the hinge region binding of the 4NH<sub>2</sub> group of **1** with Glu915 (C=O); N3 with Cys917 (N-H); 2NH<sub>2</sub> with Cys917 (C=O). The 5-thiophenyl ring lies in hydrophobic region 1 and interacts with Val897, Leu1033, and Cys1043. Thus molecular modeling supports the inhibition of VEGFR-2 by **1**.

There is currently no crystal structure of PDGFR- $\beta$  bound to a ligand. Using the structure of colony-stimulating factor-1 receptor (cFMS) (PDB 1PKG, chain A)<sup>56</sup> as the template, a homology model of inactive PDGFR- $\beta$  was generated using the Molecular Operating Environment (MOE 2007.09)<sup>57</sup> suite and methods indicated in the literature.<sup>58–60</sup> A conformational database was built for **1** and minimized and docked into the homology-modeled active site shown in Figure 8. The docked poses were then ranked. The 2- and 4-NH<sub>2</sub> groups of **1** form hydrogen bonds with the backbone residues of the hinge

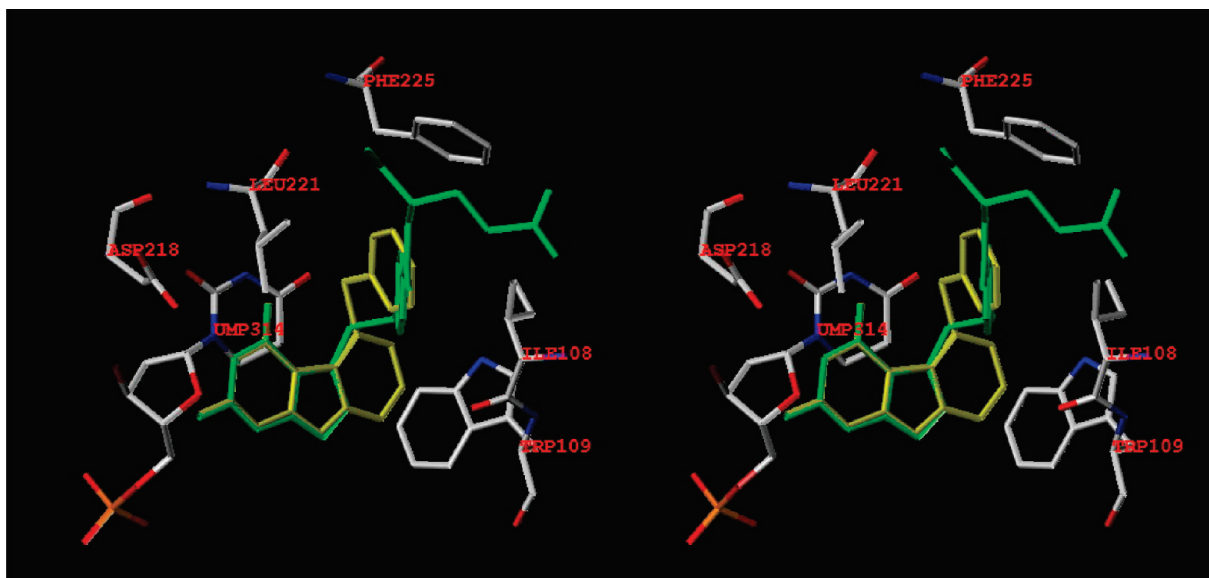


**Figure 6.** Stereoview (SYBYL7.3) of **1** superimposed on the X-ray crystal structure of pemetrexed (green) in hTS. (PDB ID 1JU6).<sup>54</sup>

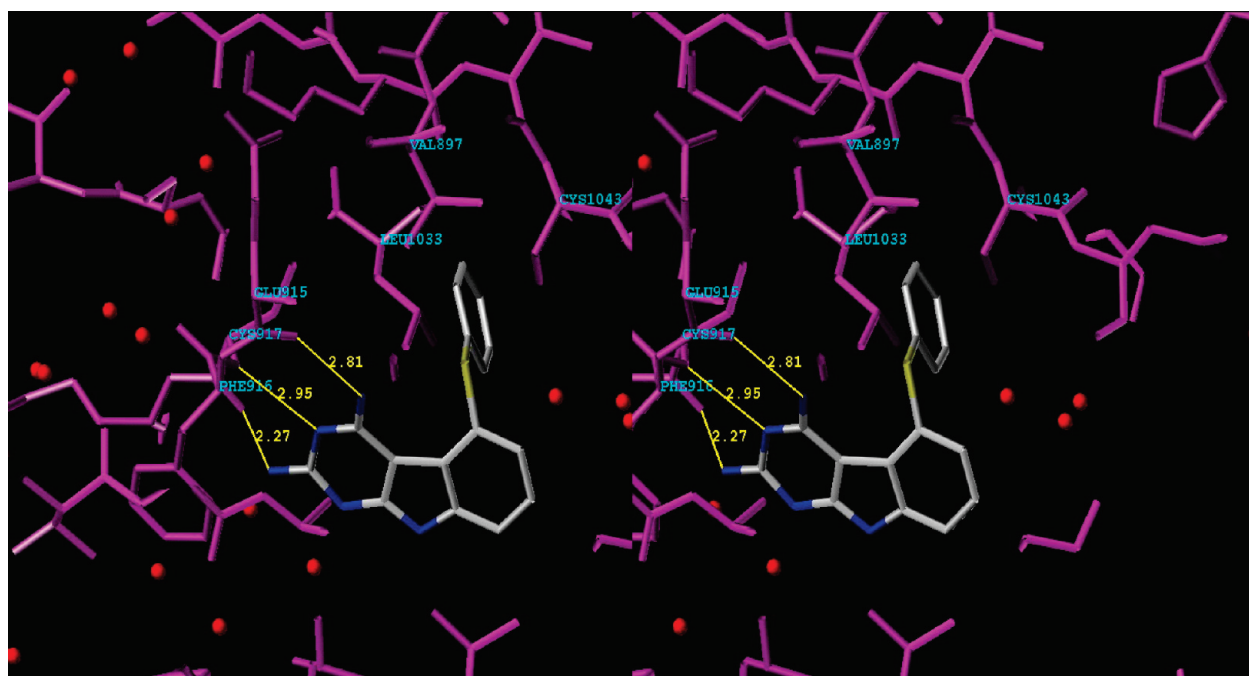


**Figure 7.** Stereoview (SYBYL7.3) of **1** superimposed on furo[2,3-*d*]pyrimidine X-ray crystal structure (not shown) in VEGFR2. Hinge region, 4NH<sub>2</sub>-Glu915 (C=O), N3-Cys917 (N-H), 2NH<sub>2</sub>-Cys917 (C=O); hydrophobic region 1, 5-thiophenyl-(Leu1033, Cys1043) (PDB ID 1YWN).<sup>55</sup>

region (Tyr683, Cys684). Additionally, the 5-S-Ph is involved in a cation- $\pi$  interaction (10–15 kcal/mol stabilization) with the protonated Arg604. Figure 8 shows only one of the low-energy binding poses of **1** with PDGFR- $\beta$  and provides a working model for binding to PDGFR- $\beta$ .

Thus we anticipated that the synthesis and evaluation of **1** and **2** would afford VEGFR-2 or PDGFR- $\beta$  inhibition or both and that these compounds would also possess DHFR or TS inhibitory activity or both, thus providing combination chemotherapy potential in single molecules.

### Chemistry

The synthesis of the target compounds is outlined in Scheme 1. Condensation of 1,2-dichloro-3-nitro-benzene **4**

with the potassium salt of ethyl cyanoacetate anion provided adduct 2-(2-chloro-6-nitrophenyl)-2-cyanoacetate **5**. Zinc dust reduction of **5**, utilizing literature conditions,<sup>39</sup> furnished ethyl 2-amino-4-chloro-1*H*-indole-3-carboxylate **6**. Cyclocondensation of **6** with carbamimidic chloride hydrochloride<sup>61</sup> afforded 2-amino-5-chloro-3*H*-pyrimido[4,5-*b*]indol-4(9*H*)-one **7**. Protection of the 2-amino group of **7** using 2,2-dimethyl propanoic anhydride provided **8**. The 4-chloro derivative **9** was prepared by treating **8** with phosphorus oxychloride at reflux. Displacement of the 4-chloro group with ammonia and concomitant deprotection of the 2-amino group of **9** was achieved by means of a sealed vessel reaction; thus the 2,4-diamino compound **10** was obtained as the common intermediate. Treatment of **10** with the appropriate

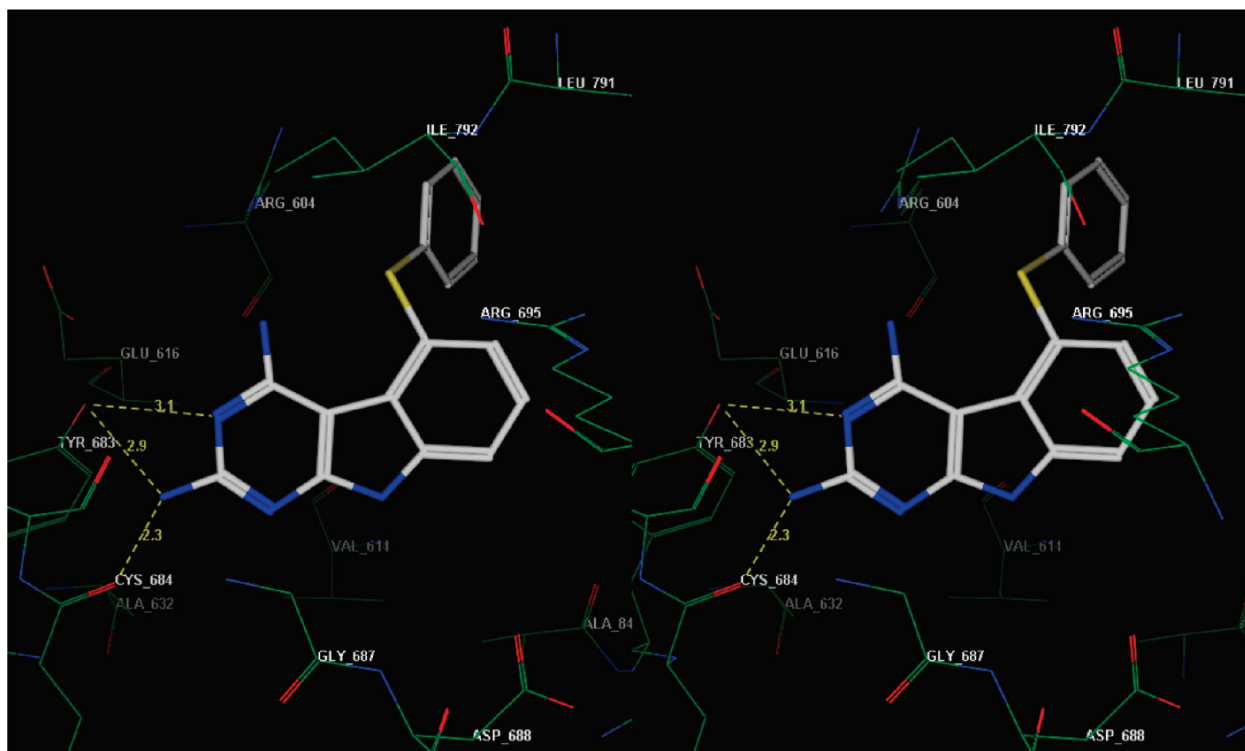
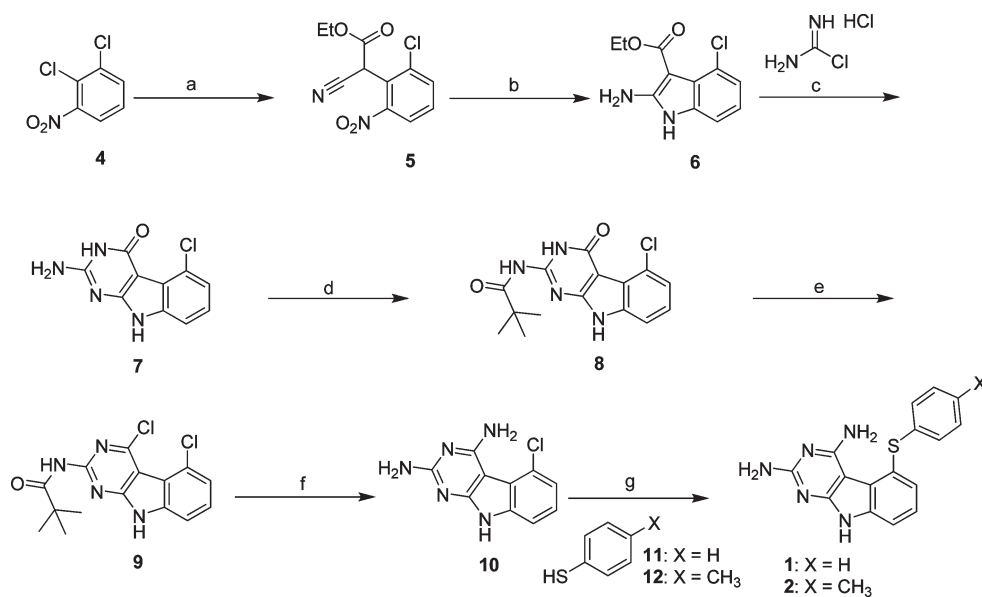


**Figure 8.** Stereoview of a docked pose of **1** in the putative PDGFR- $\beta$  active site model.

#### Scheme 1<sup>a</sup>



<sup>a</sup> Reagents and conditions: (a) EtO<sub>2</sub>CCH<sub>2</sub>CN, *t*-BuOK, THF, reflux, 48 h; (b) Zn, HOAc, 50–55 °C, 2 h, 30 min; (c) methyl sulfone, 110 °C, 30 min; (d) 2,2-dimethylpropanoic anhydride, DMAP, NEt<sub>3</sub>, DMF, 60 °C, 48 h; (e) POCl<sub>3</sub>, reflux, 4 h; (f) NH<sub>3</sub>/CH<sub>3</sub>OH, sealed vessel, 130 °C, 48 h; (g) K<sub>2</sub>CO<sub>3</sub>, NMP, microwave, 250 °C, 30 min.

substituted benzenethiols in a microwave apparatus (from Biotage) provided target compounds **1** and **2**.

#### Biological Evaluation and Discussion

Discrepancies in IC<sub>50</sub> values obtained from isolated RTK inhibitory assays compared with IC<sub>50</sub> values obtained against whole tumor cell assays are sometimes quite large (as much as 1000-fold). There are several reasons for this, and the conditions (e.g., ATP concentrations for ATP competitive agents)

of the assay dictate the IC<sub>50</sub> values. Variations in assay conditions afford different IC<sub>50</sub> values. Thus we have elected to evaluate the RTK inhibitory activity of our compounds using human tumor cells known to express high levels of the appropriate RTK.

We believe that tumor cell inhibitory assays are the most meaningful assays of the activity of the analogs evaluated and allow the most appropriate extrapolation regarding candidate selection and chances of success for *in vivo* evaluations.

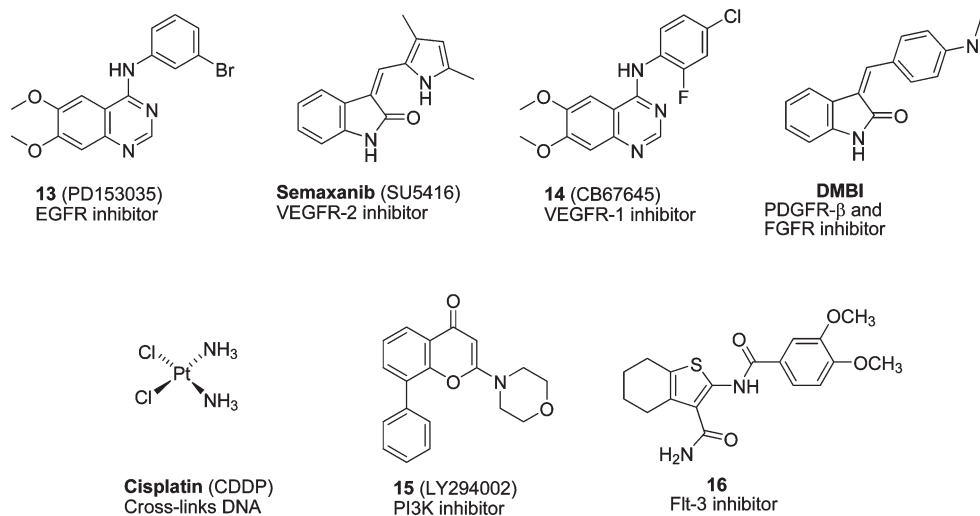


**Figure 9.** Standard drugs and control agents.

**Table 1.** IC<sub>50</sub> Values ( $\mu$ M) of Kinase Inhibition and in the A431 Cytotoxicity Assay and EC<sub>50</sub> ( $\mu$ M) against PI3K<sup>a</sup>

compd no.	EGFR kinase inhibition	VEGFR-2 (Flk-1) kinase inhibition	VEGFR-1 (Flt-1) kinase inhibition	PDGFR- $\beta$ kinase inhibition	A431 cytotoxicity	PI3K activity	Flt-3 activity
<b>1</b>	15.07 $\pm$ 3.1	22.6 $\pm$ 4.5	118.1 $\pm$ 19.4	2.8 $\pm$ 0.42	49.2 $\pm$ 4.7	21.6	41.2 $\pm$ 5.7
<b>2</b>	10.41 $\pm$ 1.2	56.3 $\pm$ 7.1	160.1 $\pm$ 28.9	40.3 $\pm$ 5.1	14.1 $\pm$ 2.0	12.2	39.6 $\pm$ 4.1
<b>13</b>	0.23 $\pm$ 0.05						
semaxinib		12.9 $\pm$ 2.9					
<b>14</b>			14.1 $\pm$ 2.8				
DMBI				3.75 $\pm$ 0.31			
cisplatin					10.6 $\pm$ 3.5		
<b>15</b>						1.5	
<b>16</b>							2.9 $\pm$ 0.031

<sup>a</sup>In-cell kinase activity was assessed by a "cytoblot" developed in our laboratory using A431 cells, which overexpress EGFR, SF539 cells for PDGFR $\beta$ , U251 cells for VEGFR2, A498 cells for VEGFR1, MV 3:11 cells for Flt-3, and HeLa cells for PI3K as described in the Detailed Methods section.

In addition to this, we recognize that the IC<sub>50</sub>'s of standard compounds also vary under different assay conditions, thus we use a standard (control) compound in each of our assays. These standard compounds were evaluated side by side with our analogs and afford direct comparison of IC<sub>50</sub>'s of our analogs with the standard compounds.

Compounds **1** and **2** were evaluated as inhibitors of EGFR, VEGFR-1, VEGFR-2, PDGFR- $\beta$ , phosphatidylinositol 3-kinase (PI3K), and Flt-3 and for antiproliferative activity against the A431 tumor cell line that overexpresses EGFR. For the RTK and PI3K assays, cells overexpressing each kinase were exposed to compound followed by the ligand for each RTK as described in the Detailed Methods section. This was followed by a "cytoblot", or in-cell ELISA, developed by our laboratory for the evaluation of kinase activity.<sup>42</sup> The compounds were compared with standards *N*-(3-bromophenyl)-6,7-dimethoxyquinazolin-4-amine (**13**) for EGFR (Figure 9), semaxinib for VEGFR-2, *N*-(4-chloro-2-fluorophenyl)-6,7-dimethoxyquinazolin-4-amine (**14**) for VEGFR-1, (*Z*)-3-((4-dimethylamino)benzylidene)indolin-2-one (DMBI) for PDGFR- $\beta$ , cisplatin (CDDP) for A431, 2-morpholino-8-phenyl-4*H*-chromen-4-one (**15**) for PI3K, and 2-(3,4-dimethoxybenzamido)-4,5,6,7-tetrahydrobenzo[*b*]thiophene-3-carboxamide (**16**) for Flt-3 (Figure 9). The results are listed in Table 1. The compounds are active against VEGFR-2 and within 2–4-fold of the standard semaxinib with **1** more potent than **2**. Against PDGFR- $\beta$ , **1** is somewhat more potent than the standard DMBI and **2** is about 11-fold less potent. Against the growth of A431 tumor cells in culture **2** is similar to cisplatin while **1**

much less potent. Since neither compound is a potent EGFR inhibitor compared with standard **13**, the marginal inhibitory activity against A431 tumor cells of **1** and **2** was not surprising. The involvement of Flt-3<sup>11</sup> inhibition for both sorafenib and sunitinib in addition to other RTKs prompted the modeling of **1** in the X-ray crystal structure of Flt-3.<sup>62</sup> This afforded an excellent docked conformation, and hence we initiated the whole cell assay for Flt-3 kinase for **1** and **2** (Table 1). Compounds **1** and **2** were about 13-fold less active against Flt-3 compared with standard **16**. Due to the importance of PI3K in tumor growth,<sup>63</sup> we also evaluated **1** and **2** in the PI3K assay using **15** as the standard (Table 1); compounds **1** and **2** are 8-fold and 11-fold less active, respectively, than the standard **15** against PI3K.

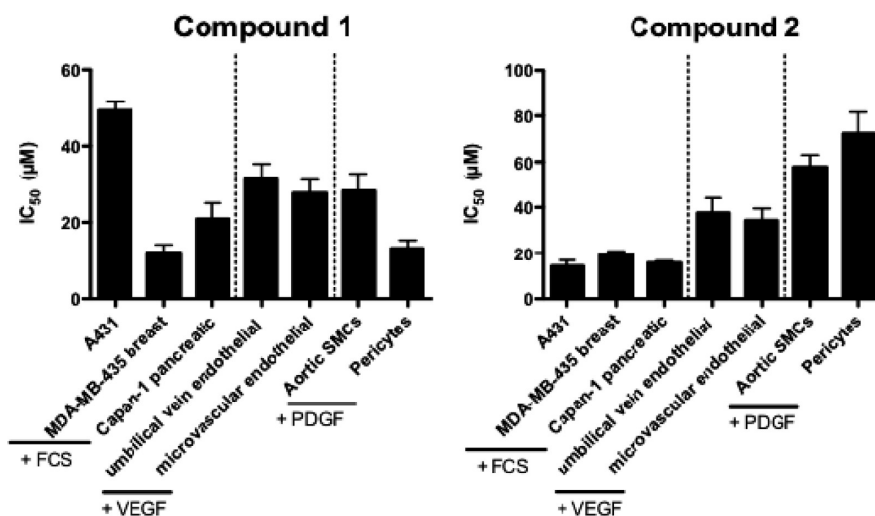
The compounds were also evaluated against isolated DHFR and TS for the cytotoxic component. The results are listed in Table 2 and are compared with standards for DHFR (MTX, trimethoprim (TMP)) and TS (PMX, RTX). The compounds were potent inhibitors of hTS at submicromolar levels that were 54-fold (**1**) and 76-fold (**2**) more active than clinically used PMX as its monoglutamate and comparable to RTX. The better hTS inhibitory activity of both **1** and **2** compared with PMX could be due to a better C-ring interaction with Trp109.

However **1** and **2** were not appreciably potent against hDHFR as well as other DHFR. Why was **1** poorly active against hDHFR? Molecular modeling had suggested that superimposition of **1** onto DHFR inhibitors in X-ray crystal structures (Figure 5) should afford inhibition of hDHFR.

**Table 2.** Inhibitory Concentrations (IC<sub>50</sub>,  $\mu$ M) against DHFR and TS

compd	TS inhibitory activity, <sup>a</sup> IC <sub>50</sub> ( $\mu$ M)			DHFR inhibitory activity, <sup>a</sup> IC <sub>50</sub> ( $\mu$ M)		
	human <sup>c</sup>	<i>Escherichia coli</i> <sup>e</sup>	<i>Toxoplasma gondii</i> <sup>d</sup>	human <sup>e</sup>	<i>Escherichia coli</i> <sup>f</sup>	<i>Toxoplasma gondii</i> <sup>d</sup>
<b>1</b>	0.54	> 27	0.11	> 33 (17) <sup>b</sup>	> 33 (35)	33
<b>2</b>	0.39	> 26	> 26	> 31 (7)	> 31 (27)	> 31 (22)
pemetrexed <sup>g</sup>	29.0	15	14			
raltitrexed <sup>h</sup>	0.29	2.3	0.48			
MTX				0.022	0.0066	0.019
trimethoprim				680	0.02	2.9

<sup>a</sup>The percent inhibition was determined at a minimum of four inhibitor concentrations within 20% of the 50% point. The standard deviations for determination of 50% points were within  $\pm 10\%$  of the value given. <sup>b</sup>Numbers in parentheses indicate the percent inhibition at the stated concentration. <sup>c</sup>Kindly provided by Dr. Frank Maley, New York State Department of Health. <sup>d</sup>Kindly provided by Dr. Karen Anderson, Yale University, New Haven, CT. <sup>e</sup>Kindly provided by Dr. Andre Rosowsky, Dana-Farber Cancer Institute, Harvard Medical School, Boston, MA. <sup>f</sup>Kindly provided by Dr. R. L. Blakley, St. Jude Children's Hospital, Memphis, TN. <sup>g</sup>Kindly provided by Dr. Chuan Shih, Eli Lilly and Co. <sup>h</sup>Kindly provided by Dr. Ann Jackman, CRC Centre for Cancer Therapeutics, Surrey SM2 5NG, England.

**Figure 10.** Cell viability assay after 48 h treatment.

The modeling provides the 5-S-phenyl of **1** in a binding mode that is at 90° to other hDHFR inhibitor (such as MTX<sup>52,53</sup> and TMQ<sup>50</sup>) side chain phenyl rings. On the basis of molecular modeling, other binding modes of **1** afford clashes of the C-ring with side chains and backbone of hDHFR. This could perhaps explain, in part, the poor activity against hDHFR.

Thus **1** and **2** were good to moderate inhibitors of VEGFR-2 and PDGFR- $\beta$ , comparable or better than the standards (except **2** for PDGFR- $\beta$ ) for RTK inhibition and potential antiangiogenic activity, and also had hTS inhibitory activity (IC<sub>50</sub>) in the submicromolar range to provide the cytotoxic effects needed for combination chemotherapy potential in single agents. The hTS IC<sub>50</sub> values were not in the single digit nanomolar range and hence should not cause severe toxicity to normal cells not compromised by the antiangiogenic effects of **1** and **2**. The usual next step is to determine the inhibitory activity against tumor cells in culture. The NCI preclinical 60 tumor panel was the obvious choice; however since angiogenesis is not part of these tumors in culture, only the cytotoxic effects were expected to play a role in the inhibition of these cells in culture. Compound **1** was evaluated against the growth of the NCI 60 tumor cell lines, and the results were as anticipated; **1** inhibited the tumors at GI<sub>50</sub> values of 1–10  $\mu$ M. This was about 10-fold less than the isolated hTS inhibitory activity (Table 2) and indicates a relatively low potency completely in keeping with the absence of the antiangiogenic component and perhaps an indication of low toxicity to normal cells.

**Pharmacodynamic (PD) Data in MDA-MB-435 Cells.** Compounds **1** and **2** were evaluated for cell viability (IC<sub>50</sub> of cell kill) in several cell types (Figure 10). In addition, MDA MB 435 metastatic dermal breast cancer cells were exposed to 20  $\mu$ M of **1** and **2** for cell cycle analysis (Figure 11), and cell signaling analysis (Figure 12) was carried out. First, cell viability was evaluated on cells serum-starved overnight before the addition of 1% FCS to the cancer cells, 200 ng/mL hrVEGF-165 to the endothelial cells, and 100 ng/mL hrPDGF-BB to the SMC variants together with drug for 24 h followed by 24 h incubation in serum-containing media and a cell viability assay carried out as described in the Experimental Section. It was found that **1** had varied effects (Figure 10) on three cancer cell lines (MDA-MB-435, A431, Capan-1) and fairly consistent effects on two endothelial cell types (HUVEC, HMEC-1). Human retinal pericytes (Huperi-3)<sup>64</sup> (not human aortic SMCs) were very sensitive to **1** cell kill (Figure 10, left panel). Compound **2** had a different profile of sensitivity than did **1** with tumor cells being the most sensitive, endothelial cells falling someplace in the middle, and SMC variants being the least sensitive to **2** (Figure 10, right panel). For cell cycle analysis, it was found that after 24 h exposure, **1** resulted in a buildup in G<sub>2</sub>/M (Figure 11, right panel) while **2** resulted in an increase in S phase (Figure 11, left panel). Next, a cell signaling experiment was performed on the MDA-MB-435 breast cells exposed for either 1 or 4 h to 20  $\mu$ M **1** or **2**. The same cells exposed to 30 J/m<sup>2</sup> UV-B for 4 h were used as a

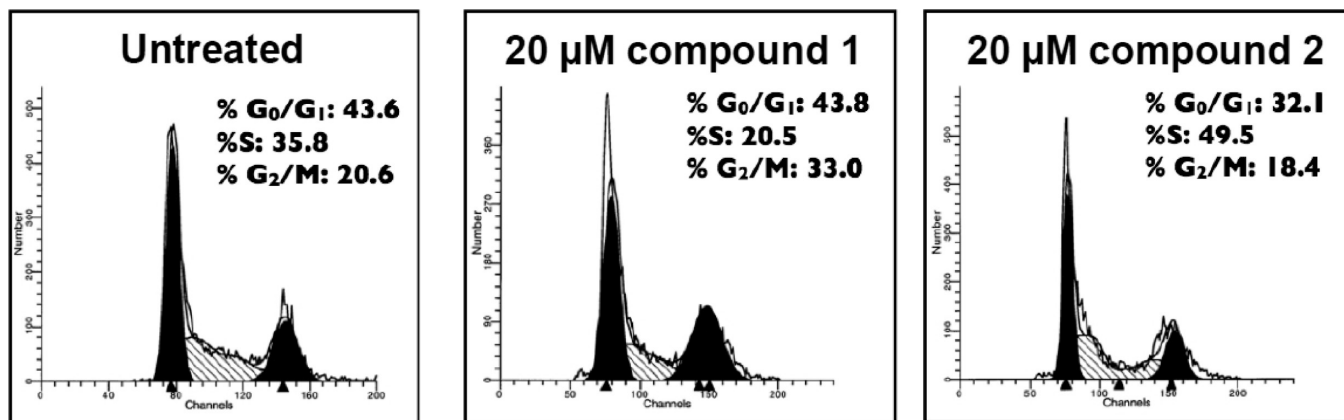


Figure 11. Cell cycle analysis.

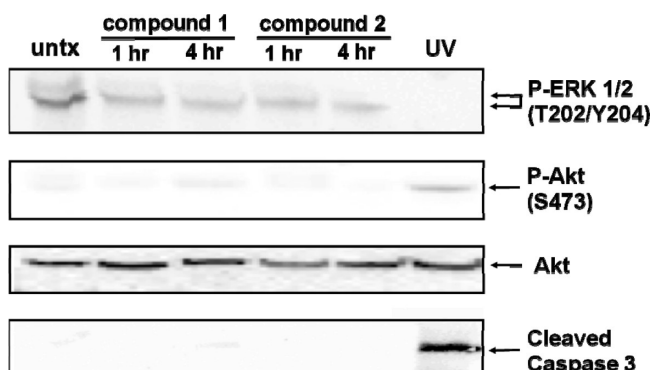


Figure 12. Cell signaling.

positive control. The first downstream target of RTKs was activated phospho-p42/44 MAPkinase (ERK 1/2), a MAP kinase member involved in cell proliferation in many cancers. It was found that both **1** and **2** reduced levels of activated ERK 1/2, but not to the same extent as UV-B exposure (Figure 12; top gel). In contrast, exposure to neither agent resulted in increased levels of activated phospho-Akt, a cell survival pathway also downstream of RTKs with levels of (nonphospho) Akt used as a loading control (Figure 12, middle two gels). Finally, neither 20 μM **1** nor 20 μM **2** resulted in increased levels of cleaved caspase 3, the terminal step in apoptosis (Figure 12; bottom most gel).

**MDA-MB-435 Chorioallantoic Membrane (CAM) Xenograft.** We have developed an intermediate systemic in vivo xenograft system using the chicken embryo CAM. This method allows for in vivo testing of more compounds in a given time and cost than the mouse tumor xenograft studies. For the CAM xenograft model, MDA-MB-435 cells (250 000) were implanted under the vascularized CAM of 10 days of incubation (DI) chicken embryos, and then the embryos were treated systemically with 25 mg/kg **1** on days one and two, and CAMs were fixed, excised, and imaged with representative images shown from five to six CAMs (Figure 13). It was found that **1** reduced both the size and the vascularity of resulting tumors, at least to the same extent as the standard VEGFR2 kinase inhibitor semaxanib at 10 mg/kg (Figure 13). These results indicate the antitumor and antiangiogenic activity of **1**. Taken together the preliminary in vitro and the in vivo results (see below) suggest that compound **1** has profound antiangiogenic activity both in vitro and in vivo. Further, these data indicate that **1** may act more on the vasculature to decrease RTK growth factor signaling

perhaps decreasing cell proliferation. The data from compound **2** are more complex; it appears that this compound acts both on the tumor and on cells of the vasculature to decrease RTK and MAPK signaling. The increase in S phase content observed in response to **2** could indicate that cells enter into DNA synthesis but cannot exit into G<sub>2</sub>, a phenomenon consistent with TS inhibition.

The logical next step was to demonstrate antitumor activity of **1** via an in vivo animal model. Compound **1** was the first choice over **2** mainly because of its better PDGFR-β inhibitory activity. To determine the antitumor effect of **1** in vivo, athymic mice were first implanted with COLO-205 metastatic colon cancer cells, shown to overexpress PDGFR-β.<sup>65</sup> At day 9 after implantation, treatment was initiated with the PDGFR-β inhibitor DMBI<sup>66</sup> at the MTD of 15 mg/kg three times weekly and with **1** at two doses, 25 and 35 mg/kg three times weekly. Tumor growth was measured using calipers. It was found that DMBI and **1** resulted in significant decreases in primary tumor growth rate (Figure 14A,B) and that **1** resulted in a further significant decrease in tumor growth rate compared with the control compound, DMBI. At the end of the experiment, tumors were taken and stained for blood vessels. It was found that **1** at 35 mg/kg three times weekly resulted in a significant decrease in primary tumor vascularity compared with control treated animals (Figure 14C) suggesting an antiangiogenic effect in vivo. Finally, livers were stained for the presence of metastases, and it was found that **1** at both 25 and 35 mg/kg, but not DMBI, resulted in significantly reduced numbers of COLO-205 metastases to the liver (Figure 14D). TGI for **1** is 76% at 35 mg/kg in this study. No MTD was determined for **1**; doses up to 75 mg/kg were well tolerated without any visual ADRs or loss in weight. Thus in vivo compound **1** has considerable antitumor activity, antiangiogenic activity, and antimetastatic activity. Further in vitro and in vivo studies are currently underway to afford further evidence of the triple mechanism(s) of action of **1** and **2** with a triple combination of a VEGFR2, a PDGFR-β, and a hTS inhibitor as standard as well as a combination of two of these standards together to determine the mechanism of action, in vivo, of **1** and **2** responsible for the in vivo antitumor, antiangiogenic, and antimetastatic activities of **1**.

We designed, synthesized, and discovered two compounds, **1** and **2**, that inhibit VEGFR-2 and PDGFR-β in whole cells at IC<sub>50</sub> values comparable to standard compounds. In addition, **1** and **2** also inhibit isolated hTS better than the monoglutamate of clinically used PMX. Thus

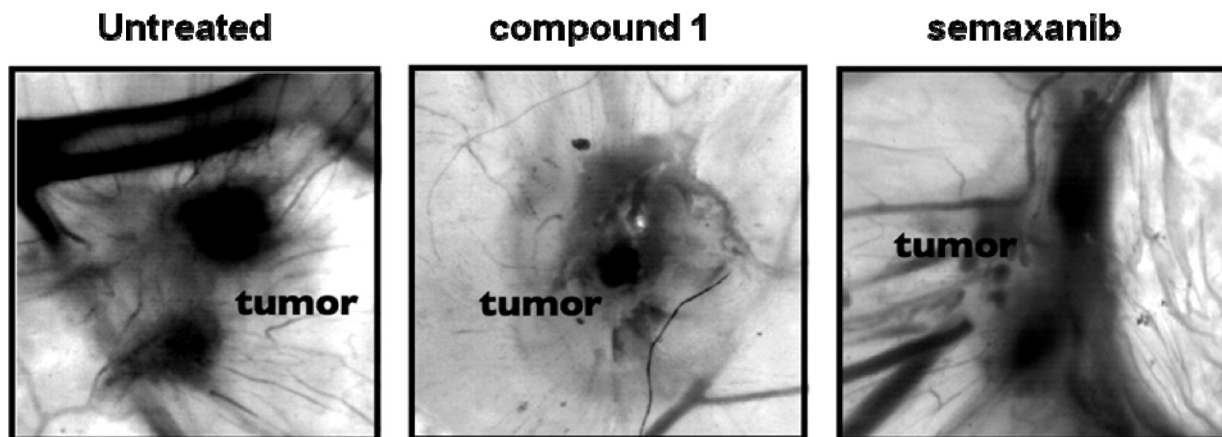


Figure 13. MDA-MB-435 CAM 72 h xenograft.

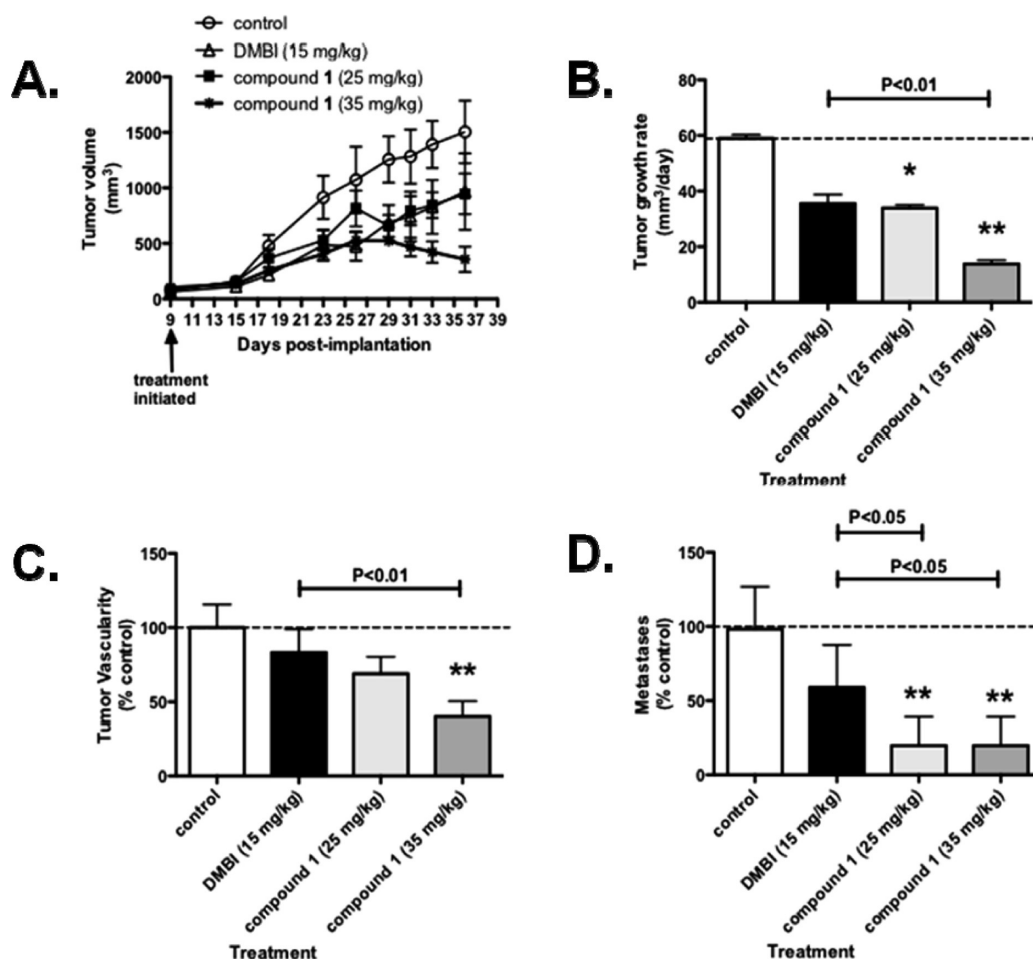


Figure 14. Tumor growth: (A) primary tumor volume, (B) primary tumor growth rate, (C) primary tumor vascularity, and (D) liver metastasis of COLO-205 tumor xenografts after various treatments. COLO-205 cells were implanted into male athymic mice as in the Detailed Methods section. Compounds were administered at the listed doses three times weekly, and tumor growth was measured using calipers. At the experiment end, tumors were stained for vascularity and livers were stained for metastases as in the Detailed Methods section. Data represent the average  $\pm$  SD of 7–11 animals: \*,  $P > 0.05$ ; \*\*,  $P < 0.01$ ; \*\*\*,  $P < 0.001$  by one-way ANOVA and Neuman–Keuls post-test. The average tumor growth rate for control treated animals (B) is 58.9 mm<sup>3</sup>/day, average number of tumor vessels in control-treated animals (C) is 11.2/field, and average metastases in control treated animals (D) are 0.65/lobe.

remarkably **1** and **2** possess both multi-RTK inhibitory activity (VEGFR-2 and PDGFR- $\beta$ ) for antiangiogenic effects and hTS inhibitory activity (cytotoxic effects) comparable to or better than clinically used single agents. Compound **1** in vivo in a COLO-205 metastatic colon cancer xenograft mouse model, at both 25 and 35 mg/kg, showed

significantly decreased tumor growth, significantly decreased liver metastasis, and significantly decreased primary tumor blood vessels (angiogenesis), remarkably without any toxicity, compared with untreated control and a standard PDGFR- $\beta$  inhibitor DMBI. The combination chemotherapeutic attributes of **1** and **2** of VEGFR-2, PDGFR- $\beta$ , and

hTS inhibitory activity makes them unique and distinct from all other known agents in clinical or investigational use. The relevance of this combination of activities in a single agent is that it mimics the clinically relevant combinations of RTK inhibitors with TS inhibitors. In addition, the *in vivo* antitumor, antiangiogenic, and antimetastatic activity of **1** supports the optimization and development of this agent and design of analogs as potential clinically useful antitumor agents that afford combination chemotherapy potential in single agents. Such single agents are designed to be used as monotherapy but could also be used with other antitumor agents or radiation as part of the therapy for cancers.

### Experimental Section

Analytical samples were dried *in vacuo* (0.2 mmHg) in a CHEM-DRY drying apparatus over P<sub>2</sub>O<sub>5</sub> at 80 °C. Melting points were determined on a MEL-TEMP II melting point apparatus with FLUKE 51 K/J electronic thermometer and are uncorrected. Nuclear magnetic resonance spectra for proton (<sup>1</sup>H NMR) were recorded on a Bruker WH-300 (300 MHz) spectrometer. The chemical shift values are expressed in ppm (parts per million) relative to tetramethylsilane as an internal standard: s, singlet; d, doublet; t, triplet; q, quartet; m, multiplet; br, broad singlet. Thin-layer chromatography (TLC) was performed on Whatman Sil G/UV254 silica gel plates with a fluorescent indicator, and the spots were visualized under 254 and 366 nm illumination. Proportions of solvents used for TLC are by volume. Column chromatography was performed on a 230–400 mesh silica gel (Fisher, Somerville, NJ) column. Elemental analyses were performed by Atlantic Microlab, Inc., Norcross, GA. Elemental compositions are within ±0.4% of the calculated values. Fractional moles of water or organic solvents frequently found in some analytical samples of antifolates could not be prevented despite 24–48 h of drying *in vacuo* and were confirmed where possible by their presence in the <sup>1</sup>H NMR spectra. Elemental analysis was used to determine the purity of the final compounds **1** and **2**. All solvents and chemicals were purchased from Aldrich Chemical Co. or Fisher Scientific and were used as received. Purity of the final compounds **1** and **2** were >95% and were determined by elemental (C, H, N, S) analysis.

**Ethyl 2-Amino-4-chloro-1H-indole-3-carboxylate (6).** To an ice-cold solution of ethyl cyanoacetate (10.9 mL, 102.4 mmol) in anhydrous THF (170 mL) under N<sub>2</sub> was added potassium *tert*-butoxide (12.07 g, 107.5 mmol). The formed white suspension was stirred for 15 min then treated with 1,2-dichloro-3-nitrobenzene **4** (9.83 g, 51.2 mmol). The suspension was heated at reflux for 48 h. The resulting reddish brown solution was poured into H<sub>2</sub>O, and the aqueous mixture was acidified to pH 2 with concentrated HCl. The mixture was extracted with ether (3×), and then the combined organic phases were dried using sodium sulfate and concentrated to give ethyl (2-chloro-2-nitrophenyl)-(cyano)acetate **5** as a dark oil. The oil was purified by column chromatography eluting with 10:1 hexane/EtOAc. TLC *R<sub>f</sub>* 0.23 (hexane/EtOAc, 3:1). <sup>1</sup>H NMR (DMSO-*d*<sub>6</sub>) δ 1.17–1.22 (t, 3 H, CH<sub>3</sub>), 4.18–4.25 (q, 2 H, CH<sub>2</sub>), 6.36 (bs, 2 H, 2-NH<sub>2</sub>, exch), 7.75–7.81 (t, *J* = 8.1 Hz, 1 H, C4-CH), 8.04–8.06 (dd, *J* = 6.9, 1.2 Hz, 1 H, Ar), 8.13–8.16 (dd, *J* = 6.9, 1.2 Hz, 1 H, Ar). The material was used directly for the next step.

A solution of impure **5** (18 g, 67 mmol) in glacial AcOH (185 mL) was treated with a single charge of Zn dust (12.1 g, 185 mmol). The mixture was heated at 55 °C for 45 min, then treated with more Zn dust (6 g). After heating for another 105 min, the mixture was filtered through a pad of Celite. The pad was washed well with AcOH, and the filtrate was concentrated to a residue that was distributed between CHCl<sub>3</sub> and H<sub>2</sub>O. The organic phase was washed with 5% aq NaHCO<sub>3</sub> and concentrated to a residue that was purified by column chromatography, eluting sequentially with 0%, 5%, and 10% EtOAc

in CHCl<sub>3</sub>. The fractions containing the pure product (TLC) were pooled and evaporated to give a pink solid. The overall yield from **4** to **6** was 63% (7.7 g of **6** was obtained). TLC *R<sub>f</sub>* 0.18 (hexane/CHCl<sub>3</sub>, 1:1); mp 140–142 °C; <sup>1</sup>H NMR (DMSO-*d*<sub>6</sub>) δ 1.26–1.30 (t, 3 H, CH<sub>3</sub>), 4.15–4.23 (q, 2 H, CH<sub>2</sub>), 6.82–6.87 (t, *J* = 7.8 Hz, 1 H, C6-CH), 6.92–6.96 (dd, *J* = 7.8 Hz, 1 H, Ar), 6.96 (bs, 2 H, 2-NH<sub>2</sub>, exch), 7.05–7.08 (dd, *J* = 7.8 Hz, 1 H, Ar), 11.35 (bs, 1 H, 9-NH, exch). Anal. (C<sub>11</sub>H<sub>11</sub>ClN<sub>2</sub>O<sub>2</sub>) C, H, N.

**2-Amino-5-chloro-3,9-dihydro-4H-pyrimido[4,5-*b*]indol-4-one (7).** A mixture of ethyl 2-amino-4-chloro-1H-indole-3-carboxylate (**6**) (200 mg, 0.837 mmol), carbamimidic chloride hydrochloride<sup>61</sup> (106.22 mg, 1.37 mmol), and methyl sulfone (1 g) was stirred and heated at 110–120 °C for 30 min. About 10 mL of water was added to quench the reaction. Ammonia–water was added to neutralize the reaction mixture. The precipitated solid was filtered, dissolved in chloroform and methanol, and dried (Na<sub>2</sub>SO<sub>4</sub>), the solvent was evaporated, and the solid was recrystallized from chloroform and methanol (1:1) in overall yield of 78%. TLC *R<sub>f</sub>* 0.33 (CHCl<sub>3</sub>/MeOH, 1:1); mp >250 °C; <sup>1</sup>H NMR (DMSO-*d*<sub>6</sub>) δ 6.58 (bs, 2 H, 2-NH<sub>2</sub>, exch), 7.04–7.06 (t, *J* = 3.3 Hz, 1 H, C7-CH), 7.17–7.20 (m, 2 H, Ar), 10.42 (s, 1 H, 3-NH, exch), 11.65 (s, 1 H, 9-NH, exch). HRMS calcd for C<sub>10</sub>H<sub>7</sub>ClN<sub>4</sub>O 234.0309, found 234.0308.

**N-(5-Chloro-4-oxo-4,9-dihydro-3H-pyrimido[4,5-*b*]indol-2-yl)-2,2-dimethyl Propanamide (8).** To a round bottomed flask were added **7** (300 mg, 1.27 mmol), 2,2-dimethylpropanoic anhydride (713.32 mg, 3.83 mmol), dimethylaminopyridine (7 mg, 0.06 mmol), and triethylamine (514.05 mg, 5.08 mmol), along with 30 mL of DMF. The mixture was stirred at 60 °C for 48 h. The DMF was removed using an oil pump to afford a residue, which was purified by column chromatography, eluting sequentially with 0%, 1%, and 5% CH<sub>3</sub>OH in CHCl<sub>3</sub>. Fractions containing the product **8** (TLC) were pooled and evaporated to give solid compound. The yield was 40% (163 mg). TLC *R<sub>f</sub>* 0.45 (CHCl<sub>3</sub>/MeOH, 10:1); mp 185.8–190.1 °C; <sup>1</sup>H NMR (DMSO-*d*<sub>6</sub>) δ 1.27 (s, 9 H, C(CH<sub>3</sub>)<sub>3</sub>), 7.18–7.21 (t, *J* = 2.4 Hz, 1 H, C7-CH), 7.24–7.26 (dd, *J* = 7.5 Hz, 1 H, Ar), 7.37–7.40 (dd, *J* = 6.3 Hz, 1 H, Ar), 11.15 (s, 1 H, 3-NH, exch), 11.93 (s, 1 H, 2-NH, exch), 12.11 (s, 1 H, 9-NH, exch). HRMS calcd for C<sub>15</sub>H<sub>15</sub>ClN<sub>4</sub>O<sub>2</sub> [M + Na]<sup>+</sup> 341.0757, found 341.0781.

**N-(4,5-Dichloro-9H-pyrimido[4,5-*b*]indol-2-yl)-2,2-dimethyl Propanamide (9).** Compound **8** (2 g, 6.274 mmol) was added to a round bottomed flask and dissolved in 30 mL of POCl<sub>3</sub>. The reaction mixture was refluxed at 110–120 °C for 4 h. After evaporation of the POCl<sub>3</sub>, ice-cold water was added. The reaction mixture was neutralized with NH<sub>3</sub>·H<sub>2</sub>O and extracted with CHCl<sub>3</sub>. The organic phase was dried with Na<sub>2</sub>SO<sub>4</sub>. The crude mixture was then purified by column chromatography, eluting sequentially with 0%, 1%, and 5% methanol in chloroform. Fractions containing the product **9** (TLC) were pooled and evaporated to give a solid. The yield was 70% (1.48 g). TLC *R<sub>f</sub>* 0.86 (CHCl<sub>3</sub>/MeOH, 5:1); mp 245.6–246.1 °C; <sup>1</sup>H NMR (DMSO-*d*<sub>6</sub>) δ 1.25 (s, 9 H, C(CH<sub>3</sub>)<sub>3</sub>), 7.36–7.39 (t, *J* = 4.5 Hz, 1 H, C7-CH), 7.49–7.51 (m, 2 H, Ar), 10.30 (s, 1 H, 9-NH, exch), 12.96 (s, 1 H, 2-NH, exch). HRMS calcd for C<sub>15</sub>H<sub>14</sub>Cl<sub>2</sub>N<sub>4</sub>O<sub>2</sub> [M + Na]<sup>+</sup> 359.0428, found 359.0442.

**5-Chloro-9H-pyrimido[4,5-*b*]indole-2,4-diamine Propanamide (10).** Compound **9** (200 mg, 0.6 mmol) was added to 5 mL of methanol saturated with ammonia. The solution was stirred at 130 °C for 2 days in a sealed vessel. The methanol was evaporated to give a solid that was purified by column chromatography, eluting sequentially with 0% and 1% methanol in chloroform. Fractions containing the product **10** (TLC) were pooled and evaporated to give a solid. The yield was 39% (54 mg). TLC *R<sub>f</sub>* 0.43 (CHCl<sub>3</sub>/MeOH, 5:1); mp 245.2–246.3 °C; <sup>1</sup>H NMR (DMSO-*d*<sub>6</sub>) δ 6.15 (bs, 2 H, 4-NH<sub>2</sub>, exch), 6.85 (bs, 2 H, 2-NH<sub>2</sub>, exch), 7.10–7.15 (t, *J* = 7.2 Hz, 1 H, C7-CH), 7.15–7.18 (dd, *J* = 9 Hz, 1 H, Ar), 7.22–7.24 (dd, *J* = 6.9 Hz, 1 H, Ar), 11.54 (bs, 1 H, 9-NH, exch). Anal. (C<sub>10</sub>H<sub>8</sub>ClN<sub>3</sub>) C, H, N, Cl.

**General Procedure for the Synthesis of 5-Substituted (Phenylthio)-9H-pyrimido[4,5-*b*]indole-2,4-diamines **1** and **2**.** Compound **10** (50 mg, 0.2 mmol), the appropriate thiol (0.9 mmol), and potassium carbonate (120 mg, 0.9 mmol) were added to a 2–5 mL biotage microwave vial. Three milliliters of NMP was added as solvent, and the tube was sealed. The reaction was run in a microwave for 30 min at 250 °C. After cooling to room temperature, the reaction mixture was transferred on top of a silica gel column and eluted with 0% and 4% methanol in chloroform. Fractions containing the product (TLC) were pooled and evaporated to afford the products **1** and **2**.

**5-(Phenylthio)-9H-pyrimido[4,5-*b*]indole-2,4-diamine (**1**).** Using the general procedure described above, the reaction of **10** with benzene thiol **11** afforded **1** as an off-white solid: yield 97% (64 mg). TLC  $R_f$  0.23 (CHCl<sub>3</sub>/MeOH 10:1); mp 251 °C; <sup>1</sup>H NMR (DMSO-*d*<sub>6</sub>) δ 6.04 (bs, 2 H, 4-NH<sub>2</sub>, exch), 7.03–7.04 (d, *J* = 4.5 Hz, 2 H, Ar), 7.13–7.16 (t, *J* = 4.2 Hz, 1 H, C7-CH), 7.21–7.27 (m, 2 H, Ar), 7.24 (bs, 2 H, 2-NH<sub>2</sub>, exch), 7.32–7.33 (dd, *J* = 4.2 Hz, 1 H, Ar), 7.40–7.42 (dd, *J* = 4.5 Hz, 1 H, Ar), 11.49 (bs, 1 H, 9-NH, exch). Anal. (C<sub>16</sub>H<sub>13</sub>N<sub>5</sub>S) C, H, N, S.

**5-(4-Methylphenylthio)-9H-pyrimido[4,5-*b*]indole-2,4-diamine (**2**).** Using the general procedure described above, the reaction of **10** with 4-methyl benzene thiol **12** afforded **2** as an off-white solid: yield 87% (60 mg). TLC  $R_f$  0.54 (CHCl<sub>3</sub>/MeOH 5:1); mp > 250 °C; <sup>1</sup>H NMR (DMSO-*d*<sub>6</sub>) δ 2.19 (s, 3 H, CH<sub>3</sub>), 6.02 (bs, 2 H, 4-NH<sub>2</sub>, exch); 7.19 (bs, 2 H, 2-NH<sub>2</sub>, exch), 6.95–6.97 (d, *J* = 6 Hz, 2 H, Ar), 7.05–7.07 (d, *J* = 6 Hz, 2 H, Ar), 7.18–7.22 (t, *J* = 6 Hz, 1 H, C7-CH), 7.29–7.31 (dd, *J* = 5.7 Hz, 1 H, Ar), 7.38–7.40 (dd, *J* = 5.7 Hz, 1 H, Ar), 11.46 (bs, 1 H, 9-NH, exch). Anal. (C<sub>17</sub>H<sub>15</sub>N<sub>5</sub>S·0.4H<sub>2</sub>O) C, H, N, S.

**Molecular Modeling.** There is currently no known crystal structure of PDGFR-β bound to a ligand. A homology model was hence built for evaluating the binding of **1** in PDGFR-β. The amino acid sequence of the PDGFR-β kinase domain was obtained from the SWISS-PROT database (ID PGFRB\_HUMAN [P09619]). As has been reported earlier in the literature,<sup>67</sup> a DISOPRED2.0<sup>68</sup> analysis of the amino acid sequence was performed to predict the ordered and disordered regions. The results from this analysis predicted amino acids 700–792 were disordered. A homology model was then built using MOE 2007.09 using the structure of c-KIT kinase complex (PDB 1PKG, chain A) as the template. A BLASTP<sup>58</sup> search indicated that chain A of the c-KIT kinase complex shows high sequence similarity with PDGFR-β (E-value: 1e-58). Sequence alignment was performed using MOE\_Align using the “actual secondary structure” option in MOE. Using the “actual secondary structure” option in MOE was necessary to correctly identify the disordered kinase insertion domain (amino acids 700–792). The final homology model returned by the program was subjected to further energy minimization using Amber99 as the forcefield and a 0.5 rms gradient. A Ramachandran plot of the model showed the presence of six outlying residues (Tyr562, Glu563, Asp590, Ser623, Ser642, Glu911). Since these residues were not in the proximity of the ATP binding site, the model was used without further refinement. Docking studies were performed using the docking suite of MOE 2007.09. After addition of hydrogen atoms, the protein was then “prepared” using the LigX function in MOE. LigX is a graphical interface and collection of procedures for conducting interactive ligand modification and energy minimization in the active site of a flexible receptor. In LigX calculations, the receptor atoms far from the ligand are constrained and not allowed to move while receptor atoms in the active site of the protein are allowed to move but are subject to tether restraints that discourage gross movement. The procedure was performed with the default settings.

Ligands were built using the molecule builder function in MOE and were energy-minimized to their local minima using the MMF94X forcefield to a constant of 0.05 kcal/mol.

Ligands were docked into the active site of the prepared protein using the docking suite as implemented in MOE.

The docking was restricted to the active site pocket residues using the Alpha triangle placement method. Refinement of the docked poses was carried out using the Forcefield refinement scheme and scored using the Affinity dG scoring system. Around 30 poses were returned for each compound at the end of each docking run. The docked poses were manually examined in the binding pocket to ensure quality of docking and to confirm absence of steric clashes with the amino acid residues of the binding pocket.

**Detailed Methods. Specific Assays. CYQUANT Cell Proliferation Marker Assay.** As a measure of cell proliferation, the CYQUANT cell counting/proliferation assay was used as previously described.<sup>69</sup> We have found that this assay is comparable in sensitivity to a clonogenic (colony-forming) assay<sup>70</sup> and lacks many of the problems associated with metabolic-based assays. For the CYQUANT assay, cells were serum-starved overnight; 1% FCS was then added along with drug to the media of cancer cells (MDA-MB-435, Capan-1, J82, A431, U251), 200 ng/mL hrVEGF-165 was added with drug to the media of endothelial cells (HUVEC, HMEC-1), and 100 ng/mL hrPDGF-BB was added to the media of SMCs (HASMCs, HuPeri-3) for 24 h; then media were replaced with fresh (drug-free) completed media for an additional 24 h. The cells were then lysed, and the CYQUANT dye, which intercalates into the DNA of cells, was added, and after 5 min, the fluorescence of each well was measured using a plate reader. A positive control used for cytotoxicity was cisplatin. Data are graphed as a percent of cells receiving no compound, and IC<sub>50</sub> values were estimated from two to three separate experiments (*n* = 6–15) using sigmoidal dose–response analysis with Prism 3.0 (GraphPad software, San Diego).

**Phosphotyrosine (PY) Cell-Based ELISA.** Because of the need for screening many compounds in multiple replicates, a higher throughput 96-well phosphotyrosine (PY) ELISA was developed.<sup>71,72</sup> Briefly, cells at 60–75% confluence were placed in serum-free medium for 18 h to reduce the background of phosphorylation. Cells used for these experiments have been shown to overexpress particular RTKs; specifically A431 for EGFR, SF539 for PDGFRβ, U251 for VEGFR2, A498 for VEGFR1, and MV 3:11 cells for Flt-3 (but not VEGFR1/2). Cells were then pretreated for 60 min with 10, 3.33, 1.11, 0.37, and 0.12 μM compound followed by an optimized dose and time of purified growth factor (EGF, PDGF-β, VEGF). The reaction was stopped, and cells were permeabilized by quickly removing the media from the cells and adding ice-cold Tris-buffered saline (TBS) containing 0.05% triton X-100, protease inhibitor cocktail, and tyrosine phosphatase inhibitor cocktail (both from Sigma Chemical). The TBS solution was then removed, and cells were fixed to the plate by heat and further incubation in 70% ethanol. Cells were further exposed to block (TBS with 1% BSA) and washed, and then a horseradish peroxidase (HRP)-conjugated phosphotyrosine antibody was added. The antibody was removed; cells were washed again and exposed to an enhanced luminol ELISA substrate, and light emission was measured using a plate reader. The known RTK-specific kinase inhibitors (PD153035, SU5416, CB67645, DMBI, and compound **16**) discussed above were used as positive controls for kinase inhibition. Data were graphed as a percent of cells receiving growth factor alone, and EC<sub>50</sub> values were estimated from two to three separate experiments (*n* = 8–24) using sigmoidal dose–response relations in Prism 3.0 software (GraphPad). In every case, the activity of a positive control inhibitor did not deviate more than 10% from the EC<sub>50</sub> values historically collected in this assay.<sup>21,42,73</sup>

**PI3 Kinase Assay.** The PI3 kinase assay is a cyto blot for the phosphorylated (active) form of the p85 subunit of PI3K. HeLa cells have been shown to possess large PI3K activity without any stimulus,<sup>74</sup> so for these studies, no inducer is necessary. HeLa cells grown in log phase for one day after passaging in serum-containing media were exposed as above to various

concentrations of unknown compounds or the known PI3K inhibitor, LY294002 for 1 h at 37 °C. As above, cells were permeabilized with Triton, fixed by heat and ethanol and blocked, and a phospho-(Tyr) p85 PI3K binding motif antibody (Cell Signaling) was added at a 1:100 dilution overnight at 4 °C. The antibody was then removed, and an anti-rabbit HRP-conjugated secondary antibody was then added (Pierce Chemical) for 30 min at RT, the antibody was removed, cells were washed again and exposed to an enhanced luminol ELISA substrate, and light emission was measured using a chemiluminescent plate reader.

**Dihydrofolate Reductase (DHFR) Assay.**<sup>75</sup> All enzymes were assayed spectrophotometrically in a solution containing 50  $\mu$ M dihydrofolate, 80  $\mu$ M NADPH, 50 mM Tris-HCl, 0.001 M 2-mercaptoethanol, and 0.001 M EDTA at pH 7.4 at 30 °C. The reaction was initiated with an amount of enzymes yielding a change in optical density at 340 nm of 0.015 units/min.

**Thymidylate Synthase (TS) Assay.** TS was assayed spectrophotometrically at 30 °C and pH 7.4 in a mixture containing 0.1 M 2-mercaptoethanol, 0.0003 M (6*R,S*)-tetrahydrofolate, 0.012 M formaldehyde, 0.02 M MgCl<sub>2</sub>, 0.001 M dUMP, 0.04 M Tris-HCl, and 0.000 75 M NaEDTA. This was the assay described by Wahba and Friedkin<sup>76</sup> except that the dUMP concentration was increased 25-fold according to the method of Davisson et al.<sup>77</sup> The reaction was initiated by the addition of an amount of enzyme yielding a change in absorbance at 340 nm of 0.016 units/min in the absence of inhibitor.

**In Vitro Pharmacodynamic Studies. Cell Cycle Analysis.** After exposure to drug, cells were fixed in 50% ethanol overnight, permeabilized, and labeled with PBS containing 0.1% Triton X-100, 100  $\mu$ g/mL Rnase A, and 25  $\mu$ g/mL propidium iodide for 45 min to 1 h at 37 °C before being subjected to flow cytometry as previously described.<sup>70</sup> Cell cycle analysis of mean fluorescence data was performed using MODFIT software to generate percent S phase, G1/G0 phase, and G2/M phase (Verity Software, Topsham, ME). Aphidicolin (250 ng/mL), an agent that inhibits DNA polymerase, was used as a control for G1 arrest,<sup>78</sup> and 50 ng/mL nocodazole, a reversible mitotic spindle poison, was used as a control for G2/M arrest (data not shown).<sup>79</sup>

**Cell Signaling Analysis.** Cells were treated with compounds at around the IC<sub>50</sub> dose for 1 and 4 h, and whole cell lysates were prepared using M-PER reagent (Pierce Chemical, Rockford, IL) with 300 mM NaCl to lyse the nucleus. Western blots against phosphorylated (activated) (ERK1/2 (Cell Signaling cat. no. 4370)) and against phospho (Cell Signaling cat. no. 4060) and nonphosphorylated Akt (Cell Signaling cat. no. 2920), two major signaling pathways downstream of RTKs, were done per manufacturer's instructions. Additionally, cleaved caspase 3 (Cell Signaling cat. no. 9661) was assessed as a marker of apoptosis.

**Chorioallantoic Membrane (CAM) Xenograft Assay.** The procedure used was a modification of a previously published procedure<sup>80</sup> Fertile Leghorn chicken eggs (CBT Farms, Chestertown, MD) were incubated until 10 DI, eggs were candled for viability, then a small window was made in the superior shell to expose the chorion and CAM. The CAM was then candled to visualize the vasculature, and a small mark was made on the chorion in a location away from major vessels. Human MDA-MB-435 cancer cells (American Type Culture Collection, Manassas, VA), 250 000 in 50  $\mu$ L of inert extracellular matrix (Humatrix, Care-Tech Laboratories, St Louis, MO), were implanted just under the CAM using a 1 mL syringe with a 25G needle. Neomycin-polymyxin ointment was then applied to the injection site, and the shell hole was covered with Micropore surgical tape (3M, St. Paul, MN). Four hours and 48 h after tumor implantation, the tape was partially removed and drug or solvent (DMSO in SWFI) was placed onto the chorion using a micropipettor, yielding a systemic dose to the embryo. In an initial dose-finding experiment, either semaxanib or compound

**1** were given at doses of 2.5, 5, 10, 15, 25, and 35 mg/kg embryo body weight<sup>81</sup> and at 3 days after injection embryo lethality was evaluated. It was found that 10 mg/kg of gemcitabine and 25 mg/kg of compound **1** were the highest doses resulting in no lethality or overt toxicity in embryos; thus these doses were used in subsequent experiments. Three days after tumor implantation, CAMs were fixed in situ by pipetting on a solution of 0.1% Triton X-100 in 4% paraformaldehyde for 1 min. The solution was removed and CAM/chorion were excised in an area surrounding the tumor implantation site. The CAM/chorion were placed into 4% paraformaldehyde and allowed to fix an addition 2 min, and the chorion was separated from the CAM. CAMs were removed to 6-well plates containing 4% paraformaldehyde. CAMs were spread gently to remove wrinkles, and images were captured at 6.25 $\times$  magnification using a brightfield dissecting microscope (Wild M400 photomakroskop, Bern, Switzerland) connected to a cooled camera (QImaging, Burnaby, BC, Canada). Images were then converted to gray scale, the number of vessels surrounding the tumor was manually counted, and the size of the tumor was determined using NIH Image J densitometry software.

**Animal Numbers.** Consulting with the Biostatistics Program at OUHSC and using StatMate software (www.graphpad.com) and a power analysis, we have found that a sample size of 10 animals is optimal for 80% power, a significance level of 0.05 in a (two-tailed) unpaired *t* test, and an expected SD of 24 (from previous experiments). Four animals per treatment group are used for short-term toxicity studies, and five animals per group are used for the longer term toxicity studies.

**Whole Animal Toxicity Assay.** To first determine the maximal tolerated dose (MTD) of a drug, male NCr nu/nu mice at 8 weeks of age without tumors were injected with 5, 10, 12.5, 15, 17.5, and 20 mg/kg compound **1** or the PDGFR- $\beta$  kinase inhibitor DMBI three times weekly, on Monday morning, Wednesday noon, and Friday afternoon. Weights were taken, and animals were observed for acute distress during the first 96 h after injection and in a 3 and 6 week period. Significance in weights was calculated after each weighing using one-way ANOVA and Neuman-Keuls post-test with the null hypothesis rejected if *P* < 0.05. Animals with significant (> 7%) weight loss were humanely euthanized and inspected for any overt toxicity, and organs (heart, lung, kidney, liver, colon) were removed for inspection by a veterinarian pathologist at OUHSC.

**COLO-205 Human Metastatic Colon Mouse Xenograft.** It has been shown that the natural killer (NK) T cell activity in athymic mice affects the metastasis of human tumor xenografts.<sup>82,83</sup> Thus for these experiments, NIH-III nude mice, deficient in NK cells, were used. One million COLO-205 (liver colonizing; ATCC) human metastatic colon cancer cells were injected subcutaneously (SQ) in the lateral flank of athymic NIH-III male mice, 8 weeks in age. Animals are monitored every other day for the presence of tumors. At the time in which most tumors are measurable by calipers (day 9 after implantation), animals with tumors were randomly sorted into treatment groups. DMSO stocks (30 mM) of drugs were further dissolved into sterile water for injection, and the optimal dose (from toxicity studies) was injected intraperitoneally (IP). The length (long side), width (short side), and depth of the tumors were measured using digital Vernier calipers each Monday, Wednesday, and Friday. Tumor volume was calculated using the formula length  $\times$  width  $\times$  depth. Tumor growth rate was then calculated using a linear regression analysis algorithm with the software Graph-Pad Prism 4.0.c. At the experiment's end, animals were humanely euthanized, tumors and liver were excised, fixed in 20% neutral buffered formalin for 8–10 h, and embedded into paraffin, and hematoxylin–eosin (H&E) stain of three separate tissue sections was completed to span the tumor and liver. Together with the OUHSC Department of Pathology core, metastases per liver lobe were counted using the H&E stained sections. The metastases can be seen as purple clusters of disorganized cells on the

highly organized largely pink liver. Together with the OUHSC Department of Pathology core, blood vessels per unit area on primary tumors were also counted in five fields at 100× magnification and averaged. Tumor growth rate per day, tumor vascularity, and liver metastases were calculated, and significance was determined from the growth curves using two-way ANOVA with a repeated measures post-test, and the null hypothesis was rejected if  $P < 0.05$ .

**Acknowledgment.** This work was supported, in part, by a grant from the National Institutes of Health, National Cancer Institute (Grant CA136944 (A.G.)).

**Supporting Information Available:** Results from elemental analysis and high-resolution mass spectrometry. This material is available free of charge via the Internet at <http://pubs.acs.org>.

## References

- Davis, D. W.; Herbst, R. S.; Abbruzzese, J. L. *Antiangiogenic Cancer Therapy*; CRC Press, Taylor and Francis Group: Boca Raton, FL: 2008; p 841.
- Folkman, J. *Angiogenesis*. *Annu. Rev. Med.* **2006**, *57*, 1–18.
- Fabbro, D.; McCormick, F., Eds. *Protein Tyrosine Kinases: From Inhibitors to Useful Drugs*; Humana Press, Totowa, NJ, 2006; 290 pp.
- Gschwind, A.; Fischer, O. M.; Ullrich, A. Timeline: The discovery of receptor tyrosine kinases: Targets for cancer therapy. *Nat. Rev. Cancer* **2004**, *4*, 361–370.
- Carmeliet, P.; Jain, R. K. Angiogenesis in cancer and other diseases. *Nature* **2000**, *407*, 249–257.
- Gorre, M. E.; Mohammed, M.; Ellwood, K.; Hsu, N.; Paquette, R.; Rao, P. N.; Sawyers, C. L. Clinical resistance to STI-571 cancer therapy caused by BCR-ABL gene mutation or amplification. *Science* **2001**, *293*, 876–880.
- Gorre, M. E.; Sawyers, C. L. Molecular mechanisms of resistance to STI571 in chronic myeloid leukemia. *Curr. Opin. Hematol.* **2002**, *9*, 303–307.
- Hurwitz, H.; Fehrenbacher, L.; Novotny, W.; Cartwright, T.; Hainsworth, J.; Heim, W.; Berlin, J.; Baron, A.; Griffing, S.; Holmgren, E.; Ferrara, N.; Fyfe, G.; Rogers, B.; Ross, R.; Kabbinavar, F. Bevacizumab plus irinotecan, fluorouracil, and leucovorin for metastatic colorectal cancer. *N. Engl. J. Med.* **2004**, *350*, 2335–2342.
- Oestman, A. PDGF receptors—mediators of autocrine tumor growth and regulators of tumor vasculature and stroma. *Cytokine Growth Factor Rev.* **2004**, *15*, 275–286.
- Pearson, M.; Garcia-Echeverria, C.; Fabbro, D. Protein Tyrosine Kinases as Targets for Cancer and Other Indications in Protein Tyrosine Kinases. In *From Inhibitors to Useful Drugs*; Fabbro, D., McCormick, F., Eds.; Human Press, Totowa, NJ, 2005, pp 1–29.
- Stein, M. N.; Flaherty, K. T. CCR drug updates: Sorafenib and sunitinib in renal cell carcinoma. *Clin. Cancer Res.* **2007**, *13*, 3765–3770.
- Tabernero, J. The role of VEGF and EGFR inhibition: Implications for combining anti-VEGF and anti-EGFR agents. *Mol. Cancer Res.* **2007**, *5*, 203–220.
- Jain, R. K.; Duda, D. G.; Clark, J. W.; Loeffler, J. S. Lessons from phase III clinical trials on anti-VEGF therapy for cancer. *Nat. Clin. Pract. Oncol.* **2006**, *3*, 24–40.
- Slamon, D. J.; Leyland-Jones, B.; Shak, S.; Fuchs, H.; Paton, V.; Bajamonde, A.; Fleming, T.; Eiermann, W.; Wolter, J.; Pegram, M.; Baselga, J.; Norton, L. Use of chemotherapy plus a monoclonal antibody against HER2 for metastatic breast cancer that overexpresses HER2. *N. Engl. J. Med.* **2001**, *344*, 783–792.
- Bergers, G.; Song, S.; Meyer-Morse, N.; Bergsland, E.; Hanahan, D. Benefits of targeting both pericytes and endothelial cells in the tumor vasculature with kinase inhibitors. *J. Clin. Invest.* **2003**, *111*, 1287–1295.
- Carmeliet, P. Angiogenesis in life, disease and medicine. *Nature* **2005**, *438*, 932–936.
- Gasparini, G.; Longo, R.; Fanelli, M.; Teicher, B. A. Combination of antiangiogenic therapy with other anticancer therapies: Results, challenges, and open questions. *J. Clin. Oncol.* **2005**, *23*, 1295–1311.
- Casanovas, O.; Hicklin, D. J.; Bergers, G.; Hanahan, D. Drug resistance by evasion of antiangiogenic targeting of VEGF signaling in late-stage pancreatic islet tumors. *Cancer Cell* **2005**, *8*, 299–309.
- Mancuso, M. R.; Davis, R.; Norberg, S. M.; O'Brien, S.; Sennino, B.; Nakahara, T.; Yao, V. J.; Inai, T.; Brooks, P.; Freemark, B.; Shalinsky, D. R.; Hu-Lowe, D. D.; McDonald, D. M. Rapid vascular regrowth in tumors after reversal of VEGF inhibition. *J. Clin. Invest.* **2006**, *116*, 2610–2621.
- Ma, J.; Waxman, D. J. Combination of antiangiogenesis with chemotherapy for more effective cancer treatment. *Mol. Cancer Ther.* **2008**, *7*, 3670–3684.
- Gangjee, A.; Zeng, Y.; Inhat, M.; Warnke, L. A.; Green, D. W.; Kisluk, R. L.; Lin, F.-T. Novel 5-substituted, 2,4-diaminofuro-[2,3-d]pyrimidines as multireceptor tyrosine kinase and dihydrofolate reductase inhibitors with antiangiogenic and antitumor activity. *Bioorg. Med. Chem.* **2005**, *13*, 5475–5491.
- Fukumura, D.; Jain, R. K. Tumor microvasculature and micro-environment: Targets for anti-angiogenesis and normalization. *Microvasc. Res.* **2007**, *74*, 72–84.
- Browder, T.; Butterfield, C. E.; Kraling, B. M.; Shi, B.; Marshall, B.; O'Reilly, M. S.; Folkman, J. Antiangiogenic scheduling of chemotherapy improves efficacy against experimental drug-resistant cancer. *Cancer Res.* **2000**, *60*, 1878–1886.
- Ferrara, N.; Kerbel, R. S. Angiogenesis as a therapeutic target. *Nature* **2005**, *438*, 967–974.
- Klement, G.; Baruchel, S.; Rak, J.; Man, S.; Clark, K.; Hicklin, D. J.; Bohlen, P.; Kerbel, R. S. Continuous low-dose therapy with vinblastine and VEGF receptor-2 antibody induces sustained tumor regression without overt toxicity. *J. Clin. Invest.* **2000**, *105*, R15–R24.
- Ho, Q. T.; Kuo, C. J. Vascular endothelial growth factor: Biology and therapeutic applications. *Int. J. Biochem. Cell Biol.* **2007**, *39*, 1349–1357.
- Lindahl, P. J. B. R.; Levéen, P.; Betsholtz, C. Pericyte Loss and Microaneurysm Formation in PDGF-B-Deficient Mice. *Science* **1997**, *277* (5323), 242–245. Sjöblom, T. P., K.; Östman, A. H. Platelet-derived growth factor. Normal function, role in disease and application of PDGF antagonists. In *Protein Tyrosine Kinases: From Inhibitors to Useful Drugs*; Fabbro, D., McCormick, F., Eds.; Humana Press, Totowa, NJ, 2006; pp 161–186.
- Clinical Trials: Combination of Capecitabine with Kinase Inhibitors: Capecitabine (Xeloda) and Lapatinib (Tykerb) as First-line Therapy in HER2/Neu-positive Breast Cancer. <http://www.clinicaltrials.gov/ct2/show/NCT00496366?term=capecitabine&rank=4>; <http://www.clinicaltrials.gov/ct2/show/NCT00496366?term=capecitabine&rank=4>; A study of Sunitinib in Combination with Capecitabine Compared with Capecitabine in Patients with Breast Cancer. <http://www.clinicaltrials.gov/ct2/show/NCT00435409?term=capecitabine&rank=5>; Study of Sunitinib in Combination with Cisplatin/Capecitabine or Oxaliplatin/Capecitabine in Patients with Advanced Gastric Cancer. <http://www.clinicaltrials.gov/ct2/show/NCT00555620?term=capecitabine&rank=6>; Bevacizumab, Erlotinib and Capecitabine for Locally Advanced Rectal Cancer. <http://www.clinicaltrials.gov/ct2/show/NCT00543842?term=capecitabine&rank=15>; Capecitabine/Erlotinib Followed of Gemcitabine Versus Gemcitabine/Erlotinib Followed of Capecitabine. <http://www.clinicaltrials.gov/ct2/show/NCT00440167>; A Phase I Trial of Capecitabine in Combination with Gemcitabine and Erlotinib for Advanced Pancreatic Cancer. <http://www.clinicaltrials.gov/ct2/show/NCT00480584>; Gemcitabine/Vinorelbine versus Gemcitabine/Cisplatin versus Gemcitabine/Capecitabine in Metastatic Breast Cancer. <http://www.clinicaltrials.gov/ct2/show/NCT00480597>; A Phase II Trial of Gemcitabine, Capecitabine and Bevacizumab in Metastatic Renal Cell Carcinoma. <http://www.clinicaltrials.gov/ct2/show/NCT0000523640>; Brain Mets - Capecitabine and WBRT. <http://www.clinicaltrials.gov/ct2/show/NCT00570908?term=capecitabine&rank=19>; Combination Study of Capecitabine and Erlotinib Concurrent with Radiotherapy for Non-operable Advanced Pancreatic Cancer. <http://www.clinicaltrials.gov/ct2/show/NCT00565487?term=capecitabine&rank=30>; Phase I Vandetanib Plau Capecitabine, Oxaliplatin and Bevacizumab for Metastatic Colorectal Cancer. <http://www.clinicaltrials.gov/ct2/show/NCT00532909?term=capecitabine&rank=44>; Phase I Study of Lapatinib in combination with Oxaliplatin and Capecitabine in Subjects with Advanced Colorectal Cancer. <http://www.clinicaltrials.gov/ct2/show/NCT00536809?term=capecitabine&rank=74>; Enzastaurin in combination of Capecitabine to Treat Breast Cancer. <http://www.clinicaltrials.gov/ct2/show/NCT00437294?term=capecitabine&rank=92>; Imatinib Mesylate, Gemcitabine and Capecitabine in Treating Patients with Advanced Solid Tumors. <http://www.clinicaltrials.gov/ct2/show/NCT00483366?term=capecitabine&rank=93>; Lapatinib + Capecitabine Treatment for Advanced Metastatic Breast Cancer in Women from China. <http://www.clinicaltrials.gov/ct2/show/NCT00508274?term=capecitabine&rank=101>; A Clinical Trial Comparing Efficacy and Safety of Sunitinib and Capecitabine. <http://www.clinicaltrials.gov/ct2/show/NCT00373113?term=capecitabine&rank=150>; Study for Patients with Untreated Gastric Cancer Who Will Receive Capecitabine and

- Lapatinib, <http://www.clinicaltrials.gov/ct2/show/NCT0000570908?term=capecitabine&rank=152>; EAP (Expanded Access Protocol) of Lapatinib Combined with Capecitabine in Metastatic Breast Cancer, <http://www.clinicaltrials.gov/ct2/show/NCT00338247?term=capecitabine&rank=167>; Phase I/II XP + Sorafenib in AGC, <http://www.clinicaltrials.gov/ct2/show/NCT00565370?term=capecitabine&rank=250>. A Brain Metastases in ErbB2-Positive Breast Cancer, <http://www.clinicaltrials.gov/ct2/show/NCT00437073?term=capecitabine&rank=267>; Lapatinib in Combination with Capecitabine in Japanese Patients with Metastatic Breast Cancer, <http://www.clinicaltrials.gov/ct2/show/NCT00477464?term=capecitabine&rank=309>; Clinical Trial on the Mixture of Gemcitabine, Capecitabine and Sorafenib (Bay 43-9006) in the Treatment of Patients with Renal Cell Carcinoma (RCC) (SOGUG-02-06), <http://www.clinicaltrials.gov/ct2/show/NCT00496301?term=capecitabine&rank=311>; Erlotinib, Combination Chemotherapy and Radiation Therapy in Treating Patients with Stage I or Stage II Pancreatic Cancer that can be Removed by Surgery, <http://www.clinicaltrials.gov/ct2/show/NCT00313560?term=capecitabine&rank=352>.
- (29) Tripathy, D. Capecitabine in combination with novel targeted agents in the management of metastatic breast cancer: underlying rationale and results of clinical trials. *Oncologist* **2007**, *12*, 375–389.
- (30) Clinical Trials Combination of 5-FU with Kinase Inhibitors: Bevacizumab, Erlotinib and 5-Fluorouracil with External Beam Radiation Therapy in Locally Advanced Rectal Cancer., <http://www.clinicaltrials.gov/ct2/show/NCT00307736>; Study of Erlotinib and Chemotherapy for Unresectable or Metastatic Cancer of the Esophagus and Gastric Cardia, <http://www.clinicaltrials.gov/ct2/show/NCT00591123>; Sunitinib, Irinotecan, Fluorouracil and Leucovorin in Treating Patients with Advanced Stomach Cancer or Gastroesophageal Cancer, <http://www.clinicaltrials.gov/ct2/show/NCT00524186>; A Phase I Study of Sunitinib in combination with Cisplatin and 5-Fluorouracil in Patients with Advanced Gastric Cancer, <http://www.clinicaltrials.gov/ct2/show/NCT00555672>; Oxaliplatin, Fluorouracil, Erlotinib and Radiation Therapy before Surgery and Erlotinib After Surgery in Treating Patients with Locally Advanced Cancer of the Esophagus or Gastroesophageal Junction, <http://www.clinicaltrials.gov/ct2/show/NCT00499564>; Cisplatin, Fluorouracil, Gefitinib and Radiation Therapy in Treating Patients with Locally Advanced Head and Neck Cancer, <http://www.clinicaltrials.gov/ct2/show/NCT00352105>; Study of FOLFIRI Chemotherapy with or without Sunitinib in Patients with Metastatic Colorectal Cancer, <http://www.clinicaltrials.gov/ct2/show/NCT00457691>; Docetaxel and Lapatinib with or without Combination Chemotherapy or Docetaxel and Trastuzumab with Combination Chemotherapy in Treating Women with Locally Advanced, Inflammatory or Resectable Breast Cancer, <http://www.clinicaltrials.gov/ct2/show/NCT00450892>; Chemotherapy, Radiation Therapy and Immunotherapy Prior to Surgery in Operable Esophageal Cancer, <http://www.clinicaltrials.gov/ct2/show/NCT00393068>; Combination Chemotherapy and Radiation therapy with or without Lapatinib in Treating Patients with Locally Advanced Cancer of the Larynx or Hypopharynx That Can Be Removed by Surgery, <http://www.clinicaltrials.gov/ct2/show/NCT00498953>; Lapatinib +/- Trastuzumab in addition to Standard Neoadjuvant Breast Cancer Therapy, <http://www.clinicaltrials.gov/ct2/show/NCT00524303>; Chemotherapy & Erlotinib in Treating Patients with Esophageal or Gastroesophageal Cancer That Cannot be Removed by Surgery, <http://www.clinicaltrials.gov/ct2/show/NCT0000539617>; A Phase II Study of 2 Doses of ZD6474 (Vandetanib) in combination with FOLFOX vs FOLFOX Alone for the Treatment of Colorectal Cancer, <http://www.clinicaltrials.gov/ct2/show/NCT00500292>.
- (31) Clinical Trials - Combination of Pemetrexed with Kinase Inhibitors: A Study to Find the Best Dose of SU011248 When Given with Pemetrexed, Pemetrexed and Cisplatin or Pemetrexed and Carboplatin in Patients with Advanced Solid Tumors, <http://www.clinicaltrials.gov/ct2/show/NCT00528619?term=pemetrexed&rank=1>; Efficacy Study Comparing ZD6474 in Combination with Pemetrexed and Pemetrexed Alone in 2nd Line NSCLC Patients (ZEAL), <http://clinicaltrials.gov/ct2/show/NCT00418886?term=pemetrexed&rank=2>; Docetaxel or Pemetrexed with or Without Cetuximab in Patients with Recurrent or Progressive Non-small Cell Lung Cancer, <http://www.clinicaltrials.gov/ct2/show/NCT00095199?term=pemetrexed&rank=3>; A Phase II Trial of Lapatinib (TYKERB) + Pemetrexed (ALIMTA) Versus Pemetrexed in Advanced Non-small Cell Lung Cancer, <http://www.clinicaltrials.gov/ct2/show/NCT00528281?term=pemetrexed&rank=7>; Study of Pemetrexed Versus Pemetrexed + Erlotinib as Treatment of Non-small Cell Lung Cancer, <http://www.clinicaltrials.gov/ct2/show/NCT00447057?term=pemetrexed&rank=14>; Cisplatin, Imatinib Mesylate, and Pemetrexed in Malignant Mesothelioma Patients, <http://www.clinicaltrials.gov/ct2/show/NCT00402766?term=pemetrexed&rank=17>; ZD6474 (Vandetanib) + Alimta Combo Study, <http://www.clinicaltrials.gov/ct2/show/NCT00506051?term=pemetrexed&rank=22>; Study of Enzastaurin Versus Placebo with Pemetrexed for Patients with Advanced or Metastatic Lung Cancer, <http://www.clinicaltrials.gov/ct2/show/NCT00530621?term=pemetrexed&rank=27>; Pemetrexed Disodium with or Without Sorafenib as Second-line Therapy in Treating Patients with Stage IIIB or Stage IV Non-small Cell Lung Cancer, <http://www.clinicaltrials.gov/ct2/show/NCT00454194?term=pemetrexed&rank=31>; AZD6244 Versus Pemetrexed (Alimta®) in Patients with Non-small Cell Lung Cancer, Who Have Failed One or Two Prior Chemotherapy Regimen, <http://clinicaltrials.gov/ct2/show/NCT00372788?term=pemetrexed&rank=32>; Randomized Phase III Trial of Pemetrexed vs Erlotinib in Pretreated Patients with NSCLC, <http://clinicaltrials.gov/ct2/show/NCT00440414?term=pemetrexed&rank=34>; Vatalanib and Pemetrexed Disodium in Treating Patients with Advanced Solid Tumors, <http://clinicaltrials.gov/ct2/show/NCT00390000?term=pemetrexed&rank=37>; Sorafenib Combined with Cisplatin and Etoposide or Carboplatin and Pemetrexed in Treating patients with Metastatic Solid Tumors, <http://clinicaltrials.gov/ct2/show/NCT00573690?term=pemetrexed&rank=92>; Study in Patients with Advanced Non-small Cell Lung Cancer Treated with Pemetrexed and Carboplatin Plus or Minus Sorafenib (PECASO), <http://clinicaltrials.gov/ct2/show/NCT00473486?term=pemetrexed&rank=98>; Chemotherapy for patients with Non-small Cell Lung Cancer Who Are Non-smokers, <http://clinicaltrials.gov/ct2/show/NCT00409006?term=pemetrexed&rank=152>; Phase I/II Trial of Bevacizumab, Pemetrexed and Erlotinib in Elderly Patients with Non-small Cell Lung Cancer, <http://clinicaltrials.gov/ct2/show/NCT00351039?term=pemetrexed&rank=202>; A Study to Evaluate Bevacizumab and Chemotherapy or Tarceva in Treating Recurrent or Refractory NSCLC (Non-small Cell Lung Cancer), <http://clinicaltrials.gov/ct2/show/NCT00095225?term=pemetrexed&rank=203>; A Study of Tarceva (Erlotinib) and Standard of Care Chemotherapy in Patients with Advanced, Recurrent or Metastatic Non-small Cell Lung Cancer (NSCLC), <http://clinicaltrials.gov/ct2/show/NCT00556322?term=pemetrexed&rank=206>.
- (32) Huber, P. E.; Bischof, M.; Jenne, J.; Heiland, S.; Peschke, P.; Saffrich, R.; Groene, H.-J.; Debus, J.; Lipson, K. E.; Abdollahi, A. Trimodal cancer treatment: Beneficial effects of combined anti-angiogenesis, radiation, and chemotherapy. *Cancer Res.* **2005**, *65*, 3643–3655.
- (33) Schnell, J. R.; Dyson, H. J.; Wright, P. E. Structure, dynamics, and catalytic function of dihydrofolate reductase. *Annu. Rev. Biophys. Biomol. Struct.* **2004**, *33*, 119–140.
- (34) Carreras, C. W.; Santi, D. V. The catalytic mechanism and structure of thymidylate synthase. *Annu. Rev. Biochem.* **1995**, *64*, 721–762.
- (35) Lehman, N. L. Future potential of thymidylate synthase inhibitors in cancer therapy. *Expert Opin. Invest. Drugs* **2002**, *11*, 1775–1787.
- (36) Pizzorno, G. D. R. B. Cheng, Y.-C. Pyrimidine and Purine Antimetabolites. In *Cancer Medicine*; Holland, J. F., Frei, E., III, Eds.; B. C. Decker, Inc.: Hamilton, London, 2003, pp 739–744.
- (37) Rollins, K. D.; Lindley, C. Pemetrexed: A multitargeted antifolate. *Clin. Ther.* **2005**, *27*, 1343–1382.
- (38) Clamp, A. R.; Schoeffski, P.; Valle, J. W.; Wilson, R. H.; Mareaud, S.; Govaerts, A. S.; Debois, M.; Lacombe, D.; Twelves, C.; Chick, J.; Jayson, G. C. A phase I and pharmacokinetic study of OSI-7904L, a liposomal thymidylate synthase inhibitor in combination with oxaliplatin in patients with advanced colorectal cancer. *Cancer Chemother. Pharmacol.* **2008**, *61*, 579–585.
- (39) Showalter, H. D. H.; Bridges, A. J.; Zhou, H.; Sercel, A. D.; McMichael, A.; Fry, D. W. Tyrosine kinase inhibitors. 16. 6,5,6-Tricyclic benzothieno[3,2-d]pyrimidines and pyrimido[5,4-b]- and [-4,5-b]indoles as potent inhibitors of the epidermal growth factor receptor tyrosine kinase. *J. Med. Chem.* **1999**, *42*, 5464–5474.
- (40) Traxler, P. M.; Furet, P.; Mett, H.; Buchdunger, E.; Meyer, T.; Lydon, N. 4-(Phenylamino)pyrrolopyrimidines: Potent and selective, ATP site directed inhibitors of the EGF-receptor protein tyrosine kinase. *J. Med. Chem.* **1996**, *39*, 2285–2292.
- (41) Traxler, P.; Furet, P. Strategies toward the design of novel and selective protein tyrosine kinase inhibitors. *Pharmacol. Ther.* **1999**, *82*, 195–206.
- (42) Gangjee, A.; Yang, J.; Ihnat, M. A.; Kamat, S. Antiangiogenic and antitumor agents. Design, synthesis, and evaluation of novel 2-amino-4-(3-bromoanilino)-6-benzylsubstituted pyrrolo[2,3-d]pyrimidines as inhibitors of receptor tyrosine kinases. *Bioorg. Med. Chem.* **2003**, *11*, 5155–5170.
- (43) Laufer, S. A.; Domeyer, D. M.; Scior, T. R. F.; Albrecht, W.; Hauser, D. R. J. Synthesis and biological testing of purine derivatives as

- potential ATP-competitive kinase inhibitors. *J. Med. Chem.* **2005**, *48*, 710–722.
- (44) Abu Thaher, B.; Koch, P.; Schattel, V.; Laufer, S. Role of the hydrogen bonding heteroatom–Lys53 interaction between the p38 $\alpha$  mitogen-activated protein (MAP) kinase and pyridinyl-substituted 5-membered heterocyclic ring inhibitors. *J. Med. Chem.* **2009**, *52*, 2613–2617.
- (45) Gangjee, A.; Lin, X.; Kisliuk, R. L.; McGuire, J. J. Synthesis of *N*-{4-[(2,4-Diamino-5-methyl-4,7-dihydro-3*H*-pyrrolo[2,3-*d*]pyrimidin-6-yl)thio]benzoyl}-*L*-glutamic Acid and *N*-{4-[(2-Amino-4-oxo-5-methyl-4,7-dihydro-3*H*-pyrrolo[2,3-*d*]pyrimidin-6-yl)thio]benzoyl}-*L*-glutamic Acid as Dual Inhibitors of Dihydrofolate Reductase and Thymidylate Synthase and as Potential Antitumor Agents. *J. Med. Chem.* **2005**, *48*, 7215–7222.
- (46) Rosowsky, A.; Forsch, R. A.; Freisheim, J. H.; Danenberg, P. V.; Moran, R. G.; Wick, M. M. Methotrexate analogs. 29. Effect of  $\gamma$ -aminobutyric acid spacers between the pteroyl and glutamate moieties on enzyme binding and cell growth inhibition. *J. Med. Chem.* **1986**, *29*, 1872–1876.
- (47) Gangjee, A.; Jain, H. D.; Kurup, S. Recent advances in classical and non-classical antifolates as antitumor and antiopportunistic infection agents: part I. *Anti-Cancer Agents Med. Chem.* **2007**, *7*, 524–542.
- (48) Gangjee, A.; Qiu, Y.; Li, W.; Kisliuk, R. L. Potent dual thymidylate synthase and dihydrofolate reductase inhibitors: Classical and nonclassical 2-amino-4-oxo-5-arylthio-substituted-6-methylthieno[2,3-*d*]pyrimidine antifolates. *J. Med. Chem.* **2008**, *51*, 5789–5797.
- (49) Gangjee, A.; Li, W.; Yang, J.; Kisliuk, R. L. Design, synthesis, and biological evaluation of classical and nonclassical 2-amino-4-oxo-5-substituted-6-methylpyrrolo[3,2-*d*]pyrimidines as dual thymidylate synthase and dihydrofolate reductase inhibitors. *J. Med. Chem.* **2008**, *51*, 68–76.
- (50) Cody, V.; Luft Joseph, R.; Pangborn, W.; Gangjee, A. Analysis of three crystal structure determinations of a 5-methyl-6-*N*-methylamino pyridopyrimidine antifolate complex with human dihydrofolate reductase. *Acta Crystallogr.* **2003**, *D59*, 1603–1609.
- (51) Tripos Inc., 1699 South Hanley Road, St. Louis, MO 63144.
- (52) Davies, J. F., II; Delcamp, T. J.; Prendergast, N. J.; Ashford, V. A.; Freisheim, J. H.; Kraut, J. Crystal structures of recombinant human dihydrofolate reductase complexed with folate and 5-deazafofolate. *Biochemistry* **1990**, *29*, 9467–9479.
- (53) Oefner, C.; D'Arcy, A.; Winkler, F. K. Crystal structure of human dihydrofolate reductase complexed with folate. *Eur. J. Biochem.* **1988**, *174*, 377–385.
- (54) Sayre, P. H.; Finer-Moore, J. S.; Fritz, T. A.; Biermann, D.; Gates, S. B.; MacKellar, W. C.; Patel, V. F.; Stroud, R. M. Multi-targeted antifolates aimed at avoiding drug resistance form covalent closed inhibitory complexes with human and *Escherichia coli* thymidylate synthases. *J. Mol. Biol.* **2001**, *313*, 813–829.
- (55) Miyazaki, Y.; Matsunaga, S.; Tang, J.; Maeda, Y.; Nakano, M.; Philippe, R. J.; Shibahara, M.; Liu, W.; Sato, H.; Wang, L.; Nolte, R. T. Novel 4-aminofuro[2,3-*d*]pyrimidines as Tie-2 and VEGFR2 dual inhibitors. *Bioorg. Med. Chem. Lett.* **2005**, *15*, 2203–2207.
- (56) Mol, C. D.; Lim, K. B.; Sridhar, V.; Zou, H.; Chien, E. Y. T.; Sang, B.-C.; Nowakowski, J.; Kassel, D. B.; Cronin, C. N.; McRee, D. E. Structure of a *c*-Kit product complex reveals the basis for kinase transactivation. *J. Biol. Chem.* **2003**, *278*, 31461–31464.
- (57) *Molecular Operating environment (MOE 2007.09)*, C. C. G., Inc., 1255 University Street, Suite 1600, Montreal, Quebec, Canada, H3B 3X3.
- (58) Altschul, S. F.; Koonin, E. V. Iterated profile searches with PSI-BLAST - a tool for discovery in protein databases. *Trends Biochem. Sci.* **1998**, *23*, 444–447.
- (59) Gallivan, J. P.; Dougherty, D. A. Cation- $\pi$  interactions in structural biology. *Proc. Natl. Acad. Sci. U.S.A.* **1999**, *96*, 9459–9464.
- (60) Mahboobi, S.; Uecker, A.; Sellmer, A.; Cenac, C.; Hoecher, H.; Pongratz, H.; Eichhorn, E.; Hufsky, H.; Truempler, A.; Sicker, M.; Heidel, F.; Fischer, T.; Stocking, C.; Elz, S.; Boehmer, F.-D.; Dove, S. Novel bis(1*h*-indol-2-yl)methanones as potent inhibitors of FLT3 and platelet-derived growth factor receptor tyrosine kinase. *J. Med. Chem.* **2006**, *49*, 3101–3115.
- (61) Henderson, E. A.; Bavetsias, V.; Theti, D. S.; Wilson, S. C.; Clauss, R.; Jackman, A. L. Targeting the  $\alpha$ -folate receptor with cyclopenta[*g*]quinazoline-based inhibitors of thymidylate synthase. *Bioorg. Med. Chem.* **2006**, *14*, 5020–5042.
- (62) Griffith, J.; Black, J.; Faerman, C.; Swenson, L.; Wynn, M.; Lu, F.; Lippke, J.; Saxena, K. The structural basis for autoinhibition of FLT3 by the juxtamembrane domain. *Mol. Cell* **2004**, *13*, 169–178.
- (63) Hennessy, B. T.; Smith, D. L.; Ram, P. T.; Lu, Y.; Mills, G. B. Exploiting the PI3K/AKT pathway for cancer drug discovery. *Nat. Rev. Drug Discovery* **2005**, *4*, 988–1004.
- (64) Ihnat, M. A.; Kaltreider, R. C.; Thorpe, J. E.; Green, D. E.; Kamat, C. D.; Leeper, M.; Shanner, A. C.; Warnke, L. A.; Piconi, L.; Ceriello, A. Attenuated superoxide dismutase induction in retinal cells in response to intermittent high versus continuous high glucose. *Am. J. Biochem. Biotechnol.* **2007**, *3*, 16–23.
- (65) Schroeder, M. C.; Hamby, J. M.; Connolly, C. J.; Grohar, P. J.; Winters, R. T.; Barvian, M. R.; Moore, C. W.; Boushelle, S. L.; Crean, S. M.; Kraker, A. J.; Driscoll, D. L.; Vincent, P. W.; Elliott, W. L.; Lu, G. H.; Batley, B. L.; Dahring, T. K.; Major, T. C.; Panek, R. L.; Doherty, A. M.; Showalter, H. D. Soluble 2-substituted aminopyrido[2,3-*d*]pyrimidin-7-yl ureas. Structure-activity relationships against selected tyrosine kinases and exploration of in vitro and in vivo anticancer activity. *J. Med. Chem.* **2001**, *44*, 1915–1926.
- (66) Zaman, G. J. R.; Vink, P. M. F.; van den Doelen, A. A.; Veeneman, G. H.; Theunissen, H. J. M. Tyrosine kinase activity of purified recombinant cytoplasmic domain of platelet-derived growth factor  $\beta$ -receptor ( $\beta$ -PDGFR) and discovery of a novel inhibitor of receptor tyrosine kinases. *Biochem. Pharmacol.* **1999**, *57*, 57–64.
- (67) Mori, Y.; Hirokawa, T.; Aoki, K.; Satomi, H.; Takeda, S.; Aburada, M.; Miyamoto, K.-i. Structure activity relationships of quinoxalin-2-one derivatives as platelet-derived growth factor- $\beta$  receptor (PDGF  $\beta$  R) inhibitors, derived from molecular modeling. *Chem. Pharm. Bull.* **2008**, *56*, 682–687.
- (68) Ward, J. J.; McGuffin, L. J.; Bryson, K.; Buxton, B. F.; Jones, D. T. The DISOPRED server for the prediction of protein disorder. *Bioinformatics* **2004**, *20*, 2138–2139.
- (69) Wilson, S. M.; Barsom, M. J.; Wilson, B. W.; Pappone, P. A. Purine nucleotides modulate proliferation of brown fat preadipocytes. *Cell Proliferation* **1999**, *32*, 131–140.
- (70) Maurer, B. J.; Ihnat, M. A.; Morgan, C.; Pullman, J.; O'Brien, C.; Johnson, S. W.; Rasey, J. S.; Cornwell, M. M. Growth of human tumor cells in macroporous microcarriers results in p53-independent, decreased cisplatin sensitivity relative to monolayers. *Mol. Pharmacol.* **1999**, *55*, 938–947.
- (71) Fong, T. A.; Shawver, L. K.; Sun, L.; Tang, C.; App, H.; Powell, T. J.; Kim, Y. H.; Schreck, R.; Wang, X.; Risau, W.; Ullrich, A.; Hirth, K. P.; McMahon, G. SU5416 is a potent and selective inhibitor of the vascular endothelial growth factor receptor (Flk-1/KDR) that inhibits tyrosine kinase catalysis, tumor vascularization, and growth of multiple tumor types. *Cancer Res.* **1999**, *59*, 99–106.
- (72) Stockwell, B. R.; Haggarty, S. J.; Schreiber, S. L. High-throughput screening of small molecules in miniaturized mammalian cell-based assays involving post-translational modifications. *Chem. Biol.* **1999**, *6*, 71–83.
- (73) Gangjee, A.; Namjoshi, O. A.; Yu, J.; Ihnat, M. A.; Thorpe, J. E.; Warnke, L. A. Design, synthesis and biological evaluation of substituted pyrrolo[2,3-*d*]pyrimidines as multiple receptor tyrosine kinase inhibitors and antiangiogenic agents. *Bioorg. Med. Chem.* **2008**, *16*, 5514–5528.
- (74) Rosenzweig, K. E.; Youmell, M. B.; Palayoor, S. T.; Price, B. D. Radiosensitization of human tumor cells by the phosphatidylinositol 3-kinase inhibitors wortmannin and LY294002 correlates with inhibition of DNA-dependent protein kinase and prolonged G2-M delay. *Clin. Cancer Res.* **1997**, *3*, 1149–1156.
- (75) Kisliuk, R. L.; Strumpf, D.; Gaumont, Y.; Leary, R. P.; Plante, L. Diastereoisomers of 5,10-methylene-5,6,7,8-tetrahydropteroyl-*D*-glutamic acid. *J. Med. Chem.* **1977**, *20*, 1531–1533.
- (76) Wahba, A. J.; Friedkin, M. Enzymic synthesis of thymidylate. I. Early steps in the purification of thymidylate synthetase of *Escherichia coli*. *J. Biol. Chem.* **1962**, *237*, 3794–3801.
- (77) Davison, V. J.; Sirawaraporn, W.; Santi, D. V. Expression of human thymidylate synthase in *Escherichia coli*. *J. Biol. Chem.* **1989**, *264*, 9145–9148.
- (78) Tsuda, H.; Sakaguchi, M.; Kawakita, M.; Nakazawa, S.; Mori, T.; Takatsuki, K. Alteration of cell cycle progression in human leukemia cell line (KOPM-28) induced by 12-*o*-tetradecanoylphorbol-13-acetate. *Int. J. Cell Cloning* **1988**, *6*, 209–220.
- (79) Iliakis, G.; Nusse, M. Arrest of irradiated G1, S, or G2 cells at mitosis using nocodazole promotes repair of potentially lethal damage. *Radiat. Res.* **1984**, *99*, 346–351.
- (80) Lucarelli, E.; Sangiorgi, L.; Benassi, S.; Donati, D.; Gobbi, G. A.; Picci, P.; Vacca, A.; Ribatti, D. Angiogenesis in lipoma: An experimental study in the chick embryo chorioallantoic membrane. *Int. J. Mol. Med.* **1999**, *4*, 593–596.
- (81) Romanoff, A. L. *Biochemistry of the Avian Embryo: A Quantitative Analysis of Prenatal Development*; Interscience: New York, 1967; 398 pp.
- (82) Hanna, N.; Fidler, I. J. Role of natural killer cells in the destruction of circulating tumor emboli. *J. Natl. Cancer Inst.* **1980**, *65*, 801–809.
- (83) Hanna, N.; Davis, T. W.; Fidler, I. J. Environmental and genetic factors determine the level of NK activity of nude mice and affect their suitability as models for experimental metastasis. *Int. J. Cancer* **1982**, *30*, 371–376.